Title
Regulating the cell shift of endothelial cell-like myofibroblasts in pulmonary fibrosis.

Journal
The European respiratory journal, 61(6)

ISSN
0903-1936

Authors
Wu, Xiuju
Zhang, Daoqin
Qiao, Xiaojing
et al.

Publication Date
2023-06-01

DOI
10.1183/13993003.01799-2022

Peer reviewed

Regulating the cell shift of endothelial cell-like myofibroblasts in pulmonary fibrosis

Xiuju Wu[1,5], Daoqin Zhang[2,5], Xiaojing Qiao[1], Li Zhang[1], Xinjiang Cai[1], Jaden Ji[1], Jocelyn A. Ma[1], Yan Zhao[1], John A. Belperio[3], Kristina I. Boström[1,4] and Yucheng Yao[1]

[1]Division of Cardiology, David Geffen School of Medicine at UCLA, Los Angeles, CA, USA. [2]Department of Pediatrics, Stanford University, Stanford, CA, USA. [3]Division of Pulmonary and Critical Care Medicine, Clinical Immunology, and Allergy, David Geffen School of Medicine, University of California, Los Angeles, CA, USA. [4]The Molecular Biology Institute at UCLA, Los Angeles, CA, USA. [5]These authors contributed equally to this work.

Corresponding author: Yucheng Yao (yyao@mednet.ucla.edu)

Shareable abstract (@ERSpublications)
New mouse models of pulmonary fibrosis are created to identify a previously unknown cell population that contributes myofibroblasts to pulmonary fibrosis. A small molecule is identified to redirect myofibroblasts and reduces pulmonary fibrosis. https://bit.ly/3DF6XjH

Cite this article as: Wu X, Zhang D, Qiao X, *et al*. Regulating the cell shift of endothelial cell-like myofibroblasts in pulmonary fibrosis. *Eur Respir J* 2023; 61: 2201799 [DOI: 10.1183/13993003.01799-2022].

This article has an editorial commentary: https://doi.org/10.1183/13993003.00407-2023

Received: 15 Sept 2022
Accepted: 25 Jan 2023

Abstract

Pulmonary fibrosis is a common and severe fibrotic lung disease with high morbidity and mortality. Recent studies have reported a large number of unwanted myofibroblasts appearing in pulmonary fibrosis, and shown that the sustained activation of myofibroblasts is essential for unremitting interstitial fibrogenesis. However, the origin of these myofibroblasts remains poorly understood. Here, we create new mouse models of pulmonary fibrosis and identify a previously unknown population of endothelial cell (EC)-like myofibroblasts in normal lung tissue. We show that these EC-like myofibroblasts significantly contribute myofibroblasts to pulmonary fibrosis, which is confirmed by single-cell RNA sequencing of human pulmonary fibrosis. Using the transcriptional profiles, we identified a small molecule that redirects the differentiation of EC-like myofibroblasts and reduces pulmonary fibrosis in our mouse models. Our study reveals the mechanistic underpinnings of the differentiation of EC-like myofibroblasts in pulmonary fibrosis and may provide new strategies for therapeutic interventions.

Introduction

Pulmonary fibrosis is a severe fibrotic lung disease, affecting >3 million people worldwide [1–6]. In the progression of pulmonary fibrosis, extensive fibrogenesis occurs in the interstitium of lung tissue, where it replaces normal structural components, damages alveolar units and disrupts gas exchange [1–8]. The survival time of patients with pulmonary fibrosis is quite poor due to the dramatic reduction of pulmonary function [4, 9–11]. Although the mechanism has not yet been determined, the deposition of abnormal extracellular fibrotic matrix is considered to be a key component in the progression of pulmonary fibrosis [12–20]. Recent studies have shown that several types of cells contribute to the stimulus of extracellular matrix deposition, such as alveolar type 2 epithelial cells and alveolar macrophages [21–24]. The studies reveal that these cells secrete a number of growth factors and cytokines that activate myofibroblasts, which produce aberrant compositions of extracellular fibrotic matrix, leading to pulmonary fibrosis [3].

Myofibroblasts were initially discovered in the granulation tissue during tissue repair [25, 26]. Advanced studies have observed that myofibroblasts contain the features of both fibroblasts and smooth muscle cells, and play a critical role in quickly responding and producing the collagens needed to repair a wound site [27, 28]. Beyond normal tissue repair, overloaded myofibroblasts are found in almost all fibrotic organs, including the liver [29], kidneys [30], heart [31] and lungs [1–6], where myofibroblasts persistently produce and accumulate unwanted fibrotic components to form scar tissue [16]. In pulmonary fibrosis, excessively activated myofibroblasts have been shown to generate deleterious extracellular matrix that are dominated by fibrillar collagens, fibronectin and other fibrotic proteomes [1–6, 32, 33]. Although studies

suggest that several cell lineages may be involved in the differentiation of myofibroblasts, the origin of myofibroblasts remains unclear.

Matrix Gla protein (MGP) is a bone morphogenic protein (BMP) antagonist and highly expressed in pulmonary cells [34–38]. MGP is essential for endothelial–epithelial interactions to direct pulmonary specification. Conventional deletion of the *Mgp* gene in mice causes an imbalance between the pulmonary vasculature and the airways, leading to vascular malformations and underdeveloped lungs [36, 38]. Mutations in the human *Mgp* gene cause Keutel syndrome, which is characterised by peripheral pulmonary stenoses and other developmental defects [39]. With warfarin treatment that renders MGP nonfunctional by interfering with γ-carboxylation, pulmonary fibrosis deteriorates sharply [40–42]. In addition, MGP has been found to support normal endothelial differentiation in progenitor cells and prevent endothelial cells (ECs) from unwanted differentiation [43–45].

In this article, we reveal that cell-specific deletion of *Mgp* gene causes severe pulmonary fibrosis. We identify previously unknown endogenous EC-like myofibroblasts, which can differentiate into myofibroblasts in normal lungs, and we show that EC-like myofibroblasts significantly contribute myofibroblasts to pulmonary fibrosis. We find that MGP binds to a unique member of the BMP family, BMP-1, to inhibit its activity in the differentiation of EC-like myofibroblasts. Additionally, we identify a small molecule that redirects the differentiation of EC-like myofibroblasts and reduces pulmonary fibrosis.

Material and methods

Animals

VE-cadherin^{cre} (B6.FVB-Tg(Cdh5-cre)7Mlia/J), *SM22a*^{cre} (B6.129S6-Taglntm2(cre)Yec/J) and *Rosa*^{tdTomato} (B6;129S6-Gt(ROSA)26Sortm9(CAG-tdTomato)Hze/J) mice on C57BL/6J background were purchased from the Jackson Laboratory. *VE-cadherin*$^{cre/ERT2}$ mice were obtained as gifts from Ralf Adams (Max Planck Institute for Molecular Biomedicine, Münster, Germany). Genotypes were confirmed by PCR [38], and experiments were performed with generation F4–F6. Littermates were used as wild-type controls. All mice were fed a standard chow diet (Diet 8604; Harlan Teklad Laboratory). Bleomycin (Cat# 1076308) and UK383367 (Cat# PZ0156) were obtained from MilliporeSigma. The studies were reviewed and approved by the institutional review board and conducted in accordance with the animal care guidelines set by the University of California, Los Angeles. The investigation conformed to the National Research Council *Guide for the Care and Use of Laboratory Animals* [46].

Tissue culture

The tdTomato^{-}VE^{-}cadherin^{+}, tdTomatoVE^{+}cadherin^{+} and tdTomatoVE^{+}cadherin^{-} cells were isolated using fluorescence-activated cell sorting (FACS) and cultured as described previously [47]. Berbamine (547190; Sigma-Aldrich), transforming growth factor (TGF)β1 (7666-MB; R&D Systems) and BMP-1 (RDC2450; R&D Systems) treatments were performed as described in the Results section. Lentiviral vectors containing cytomegalovirus (CMV)–activin receptor-like kinase (ALK)5, CMV-FoxA2, MGP or FoxA2 short interfering (si)RNA were all purchased from GeneCopoeia and applied to the cells as per the manufacturer's protocols.

Vector construction

The FLAG-hMGP vector was constructed as described previously [47]. Briefly, to construct the N-terminally FLAG-tagged human (h)MGP vector, a fragment containing the coding region for hMGP was amplified using PCR. The FLAG tag was placed in the N-terminus of the secreted, mature protein by subcloning a synthesised FLAG-coding DNA fragment between the coding regions of the signal peptide and the mature protein. The FLAG-containing hMGP DNA fragment was amplified using PCR and subcloned into the NheI and XhoI sites of pcDNA3.1(+) (Invitrogen) using restriction sites in the primers.

Pulmonary function tests

Mouse pulmonary function tests were performed as described previously [35]. Mice were weighed and placed into a single chamber with a volume of 0.8 L in which they were allowed to move freely and acclimate for ⩾15 min. To provide a baseline reading, a room air reading was taken as follows: compressed air was supplied to the chamber at a flow rate of 1 L·min^{-1} for 45 min. At this point, the chamber was completely sealed, with air flow momentarily stopped. The changes in pressure caused by breathing were recorded and amplified by the software. Subsequently, the mice were allowed to rest for ⩾5 min or until the breathing returned to baseline before conducting the hypercapnia phase. In the hypercapnia phase, a gas mixture containing 7% carbon dioxide (CO_2), 21% oxygen and balanced nitrogen was supplied to the chamber at a flow of 1 L·min^{-1}. After 5 min, the chamber was sealed and ventilatory patterns recorded. During the breathing room air and hypercapnia phase, the average tidal volume and respiratory rate were

measured for a period of ⩾10 consecutive breaths. To avoid an excessive build-up in CO_2 concentration within the chamber due to rebreathing, a bias flow regulator (Buxco Electronics) was used. The bias flow regulator provided a quiet, constant and smooth flow through the animal chamber, which prevented CO_2 build-up. The following parameters were recorded: respiratory rate, tidal volume, peak inspiratory flow, peak expiratory flow and minute ventilation. The results were calculated and corrected for body weight. Average values were calculated once per minute for each serial 10 min. The machine was sanitised with alcohol between uses.

RNA analysis

Real-time PCR analysis was performed as described previously [35]. Glyceraldehyde 3-phosphate dehydrogenase was used as a control gene [35]. Primers and probes for mouse MGP, Col3a1, Fibronectin 1 (Fn1), VE-cadherin, Flk1, ALK5, FoxA2 and von Willebrand factor were obtained from Applied Biosystems as part of TaqMan Gene Expression Assays.

ELISA

ELISA was performed as described previously [35]. ELISA kits were obtained from Abcam (ab119557 and ab222942). The assays were performed in accordance with the manufacturer's protocols.

Single-cell RNA-sequencing

10x library preparation, sequencing and alignment

A single-cell RNA-sequencing (scRNA-seq) library was generated with the Chromium Single Cell 3′ v3 assay (10x Genomics). The library was sequenced using Illumina NextSeq 550 platform with a depth of 378 million reads. Raw reads were aligned to the mouse genome (mm10). The cellranger (v3.0.0) mkfastq function was used to generate FASTQ files and cells and gene counts were called using the cellranger count function.

Cell clustering and cell type annotation

The R package Seurat version 4.0.1 was used for cell clustering and differential gene expression analysis. Cells were first filtered to have >500 detected genes and <10% of mitochondrial genes. Natural-log transformation was then applied to the gene counts and data were scaled to regress out total number of RNA counts and the percentage of mitochondrial reads. The "findvariablefeatures" function was used to select variable genes with default parameters and principal component analysis (PCA) was performed using the "runPCA" function on the variable genes. The first 25 principal components were used for cell clustering with a resolution of 0.5. Uniform manifold approximation and projection (UMAP) dimensional reduction was applied using the "runUMAP" function. The "findallmarkers" function was used to identify marker genes for each cluster. Cell identities were defined by known marker genes. The "findmarkers" function was performed for differential gene expression analysis between two cell types using the Wilcoxon rank sum test with at least log-fold difference of 0.25 between the two groups of cells.

Pseudotime trajectory construction

The R package Monocle (v2.18.0) was used for pseudotime trajectory construction. Genes with average expression >0.5 were retained for trajectory analysis in a subset of data. Variable genes were adopted from variable features identified by the Seurat "findvariablefeatures" function, then were used as ordering genes. The trajectory was constructed by the "reducedimension" function with default parameters. Differential expression in pseudotime was carried out by the "differentialgenetest" function using likelihood ratio tests.

CMap and compound identification

From each cell type in scRNA-seq analysis, we selected the top 100 marker genes. Connectivity Map (CMap) from the Broad Institute is a database with a collection of gene expression profiles that were obtained from nine human cell lines treated with various small compounds. To identify a small molecule from 2429 compounds in the LINCS database (L1000), we used the next-generation CMap (CLUE) platform to directly explore the connectivity of gene signatures among perturbagens with Touchstone tool. The drug similarity was ranked according to the CMap connectivity score (from −100 to 100). Connectivity scores >95 or <−95 were considered as strong scores to predict small candidate molecule corresponding to the query of selected gene expression signatures between different cell types.

FACS

FACS analysis was performed as described previously [35]. The cells were stained with fluorescein isothiocyanate (FITC)$^-$, phycoerythrin (PE)$^-$ or Alexa Fluor 488 (AF-488)$^-$ conjugated antibodies against CD34 and VE-cadherin (553731 and 562243; BD Biosciences). Nonspecific fluorochrome- and isotype-matched IgGs (BD Pharmingen) served as controls.

Immunoblotting and immunofluorescence

Immunoblotting was performed as described previously [44]. Equal amounts of tissue lysates were used for immunoblotting. Blots were incubated with specific antibodies to BMP-1 and latent TGFβ1-binding protein-1 (LTBP-1) (ab205394 and ab78294; Abcam), Flag (F3165; Sigma-Aldrich), ALK5 (MAB5871; R&D Systems), Col3a1 and Fn1 (NB600 and NBP1-91258; Novus Biologicals). β-Actin (A2228; Sigma-Aldrich) was used as a loading control. Immunofluorescence was performed as described in detail previously [44]. We used specific antibodies to CD34 (553731; BD Bioscience or ab54208; Abcam), Nkx2.1 (ab76013; Abcam) and VE-cadherin (562243; BD Biosciences). The nuclei were stained with 4′,6-diamidino-2-phenylindole (D9564; Sigma-Aldrich).

Masson's trichrome staining

Sections were deparaffinised, rehydrated and stained with Trichrome Stain Kit (ab150686; Abcam) as per the manufacturer's protocol. After being washed in distilled water, the sections were dehydrated and cleared in xylene, then mounted with resinous mounting medium.

Statistical analysis

The analyses were performed using GraphPad Instat (version 3.0; GraphPad Software). Data were analysed by either unpaired two-tailed t-test or one-way ANOVA with Tukey's multiple-comparisons test for statistical significance.

Results

Specific MGP deletion causes pulmonary fibrosis

We have shown that a conventional gene deletion of *Mgp* disrupted pulmonary cell differentiation [35, 38]. To perform cell-specific deletions of *Mgp*, we generated $Mgp^{flox/flox}$ mice, in which the genomic region of exons 2–4 of *Mgp* gene was floxed by two loxP sites (supplementary figure S1). We bred $Mgp^{flox/flox}$ mice with *VE-cadherin*^{cre} or *Smooth muscle 22*α^{cre} (*SM22*α^{cre}) mice. At 10 weeks of age, Masson's trichrome staining showed striking pulmonary fibrosis in both *VE-cadherin*$^{cre}Mgp^{flox/flox}$ mice and *SM22*$\alpha^{cre}Mgp^{flox/flox}$ mice, in which quantification of collagen in lung tissues confirmed more collagen accumulated (figure 1a and b). At 1 year of age, both groups of mice had severe pulmonary fibrosis (figure 1a and b). We examined the pulmonary function of the mice at 1 year of age using unrestricted whole-body barometric plethysmography. The results showed that the respiratory rates of *VE-cadherin*$^{cre}Mgp^{flox/flox}$ mice and *SM22*$\alpha^{cre}Mgp^{flox/flox}$ mice were significantly higher than that of $Mgp^{flox/flox}$ control mice during room air breathing and hypercapnia phases (figure 1c). In addition, *VE-cadherin*$^{cre}Mgp^{flox/flox}$ and *SM22*$\alpha^{cre}Mgp^{flox/flox}$ mice displayed a significant decrease in tidal volume and lower peaks of expiratory and inspiratory flow (figure 1c). Bleomycin-injected wild-type mice and $Mgp^{flox/flox}$ mice were used as controls [48]. The results suggested that progressive pulmonary fibrosis occurred in both *VE-cadherin*$^{cre}Mgp^{flox/flox}$ mice and *SM22*$\alpha^{cre}Mgp^{flox/flox}$ mice.

Endogenous EC-like myofibroblasts in normal lungs

Interestingly, when we examined the expression of endothelial markers, immunostaining and FACS both showed a robustly increased $CD34^+$ cell population in the lungs of *VE-cadherin*$^{cre}Mgp^{flox/flox}$ mice and *SM22*$\alpha^{cre}Mgp^{flox/flox}$ mice (figure 2a). We verified this result using different anti-CD34 antibodies (supplementary figure S2). In addition, we showed that the increase of $CD34^+$ cell population in the lungs of *VE-cadherin*$^{cre}Mgp^{flox/flox}$ mice and *SM22*$\alpha^{cre}Mgp^{flox/flox}$ mice persisted at 1 year of age (supplementary figure S2). Furthermore, immunostaining showed an increase of the $CD34^+$ cell population in human pulmonary fibrosis (figure 2b). We used Nkx2.1 staining as control and showed no overlap between $CD34^+$ cells and pulmonary epithelial cells.

We isolated the lungs of wild-type mice and used FACS to select a pulmonary $CD34^+$ population, in which immune cells were excluded. We examined the transcriptional profile of $CD34^+CD45^-$ cells at single-cell resolution. The scRNA-seq uncovered specific cell clusters in the $CD34^+CD45^-$ population (figure 3a). Differential gene expression divided these clusters into three major types of cells: 1) ECs that only expressed endothelial markers; 2) EC-like myofibroblasts that expressed endothelial and myofibroblast markers, and MGP, SM22α, Snai1, Snai2, Zeb1 and Zeb2; and 3) myofibroblasts that expressed myofibroblast markers and Twist1 and 2 (figure 3a). Cell differentiation trajectory projected a clear differential path from ECs to EC-like myofibroblasts ending with myofibroblasts (figure 3b). Interestingly, none of the clusters expressed the typical smooth muscle cell marker smooth muscle myosin heavy chain (SMMHC), ruling out the involvement of smooth muscle cells (figure 3a). We examined wild-type mouse lungs and healthy human lungs. Immunostaining showed the co-localisation of VE-cadherin and platelet-derived growth factor receptor (PDGFR)α around the vessels and small airways in the mouse lungs (figure 3c). The co-localisation was also identified in the structures of alveolar units

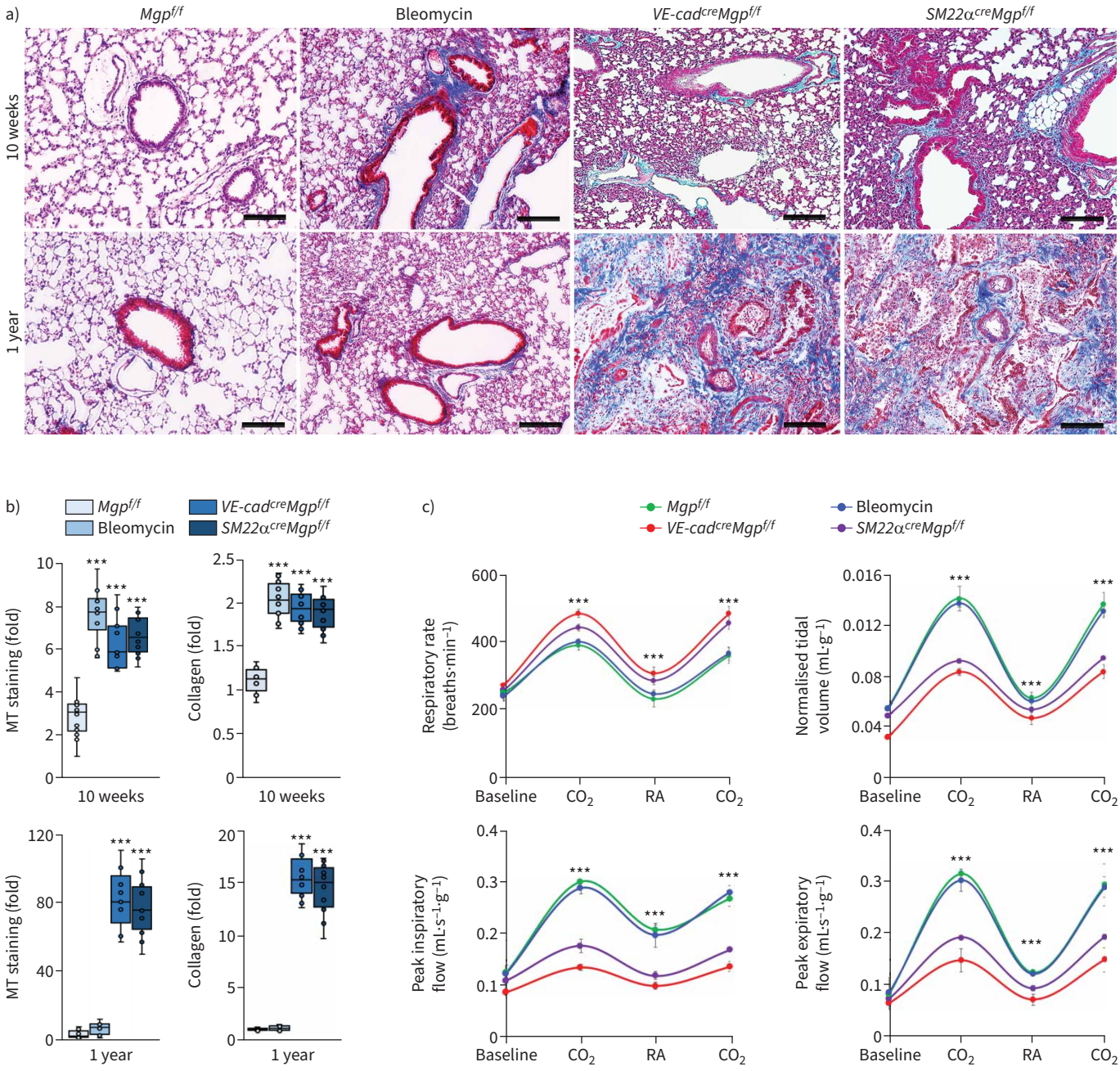

FIGURE 1 Pulmonary fibrosis in *VE-cadherin*^{cre}*Mgp*$^{flox/flox}$ and *Sm22α*^{cre}*Mgp*$^{flox/flox}$ mice. a) Masson's trichrome (MT) staining of pulmonary tissues (n=10). Scale bar=100 µm. b) Quantification of MT staining and collagen accumulation in pulmonary tissues (n=9). c) Mouse pulmonary tests (n=6). b) and c) were analysed for statistical significance by ANOVA with *post hoc* Tukey's test. The bounds of the boxes are upper and lower quartiles with data points; the line in the box is the median. In b), error bars are maximal and minimal values; in c), error bars are mean±SD. Bleomycin: wild-type mice injected with bleomycin; VE-cad: VE-cadherin; Mgp: matrix Gla protein; f/f: flox/flox; CO_2: hypercapnia phase with 7% carbon dioxide, 21% oxygen and balanced nitrogen; RA: room air. ***: p<0.0001.

in healthy human lungs (figure 3c). The results suggested that the endogenous EC-like myofibroblasts in normal lungs contribute to myofibroblasts.

We examined $CD34^{+}CD45^{-}$ cells in the lungs of *VE-cadherin*^{cre}*Mgp*$^{flox/flox}$, *SM22α*^{cre}*Mgp*$^{flox/flox}$ and bleomycin-injected wild-type mice. FACS showed an increased number of $CD34^{+}CD45^{-}$ cells in all

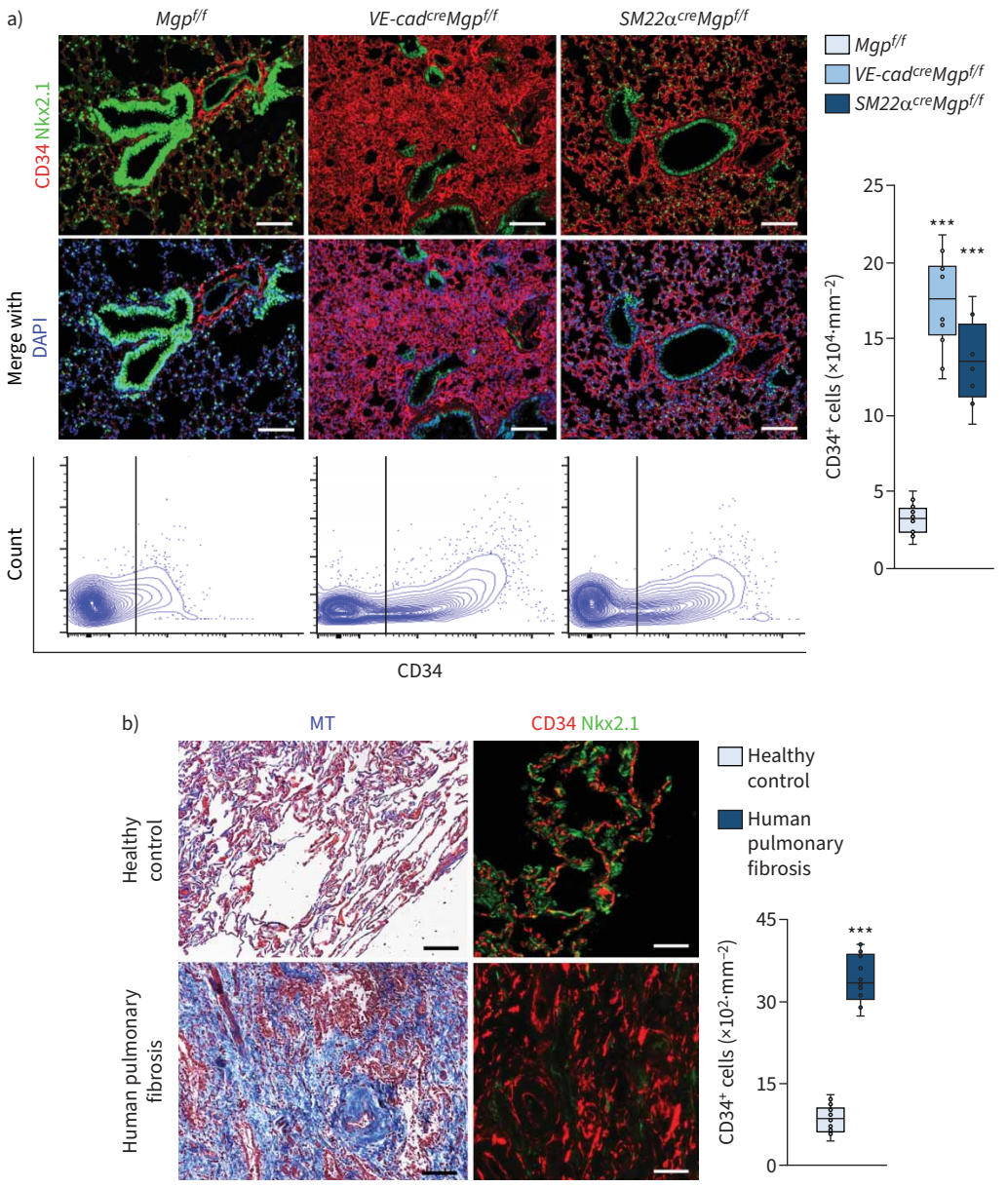

FIGURE 2 Enlarged $CD34^+$ cell population in pulmonary fibrosis. a) Immunostaining with quantification of $CD34^+$ cells and fluorescence-activated cell sorting in pulmonary tissues of *VE-cadherin*^{cre}*Mgp*$^{flox/flox}$ and *Sm22α*^{cre}*Mgp*$^{flox/flox}$ mice (n=8). *Mgp*$^{flox/flox}$ was used as control. b) Masson's trichrome (MT) staining and immunostaining of human tissues with pulmonary fibrosis and quantification of $CD34^+$ cells in human pulmonary fibrosis (n=6). Healthy lungs were used as control. Scale bars=100 µm. The data were analysed for statistical significance by unpaired two-tailed t-test; the bounds of the boxes are upper and lower quartiles with data points; the line in the box is the median; error bars are maximal and minimal values. VE-cad: VE-cadherin; Mgp: matrix Gla protein; f/f: flox/flox; DAPI: 4',6-diamidino-2-phenylindole. ***: p<0.0001.

three models (figure 3d), suggesting a similar induction of $CD34^+CD45^-$ cells in mouse models of pulmonary fibrosis.

EC-like myofibroblasts contribute to human pulmonary fibrosis

To determine the role of EC-like myofibroblasts in pulmonary fibrosis, we re-analysed publicly available scRNA-seq data of 10 healthy human lungs and 20 patients with pulmonary fibrosis [15, 32]. The analysis identified the cluster of EC-like myofibroblasts that co-expressed endothelial and myofibroblast markers, MGP and SM22α in healthy lungs and pulmonary fibrosis (figure 4a and b). Cell differential trajectory

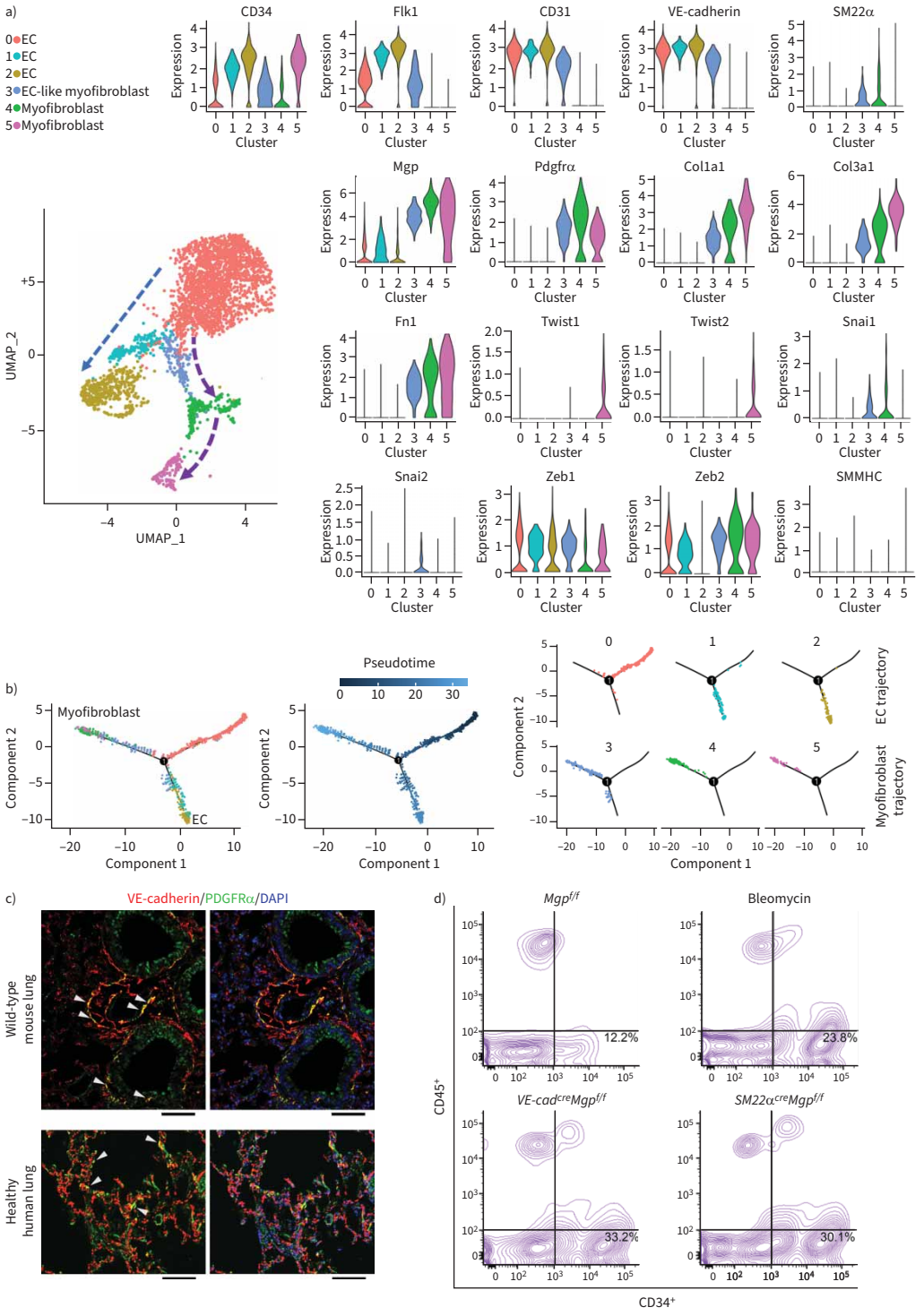

FIGURE 3 Endogenous population of endothelial cell (EC)-like myofibroblasts in wild-type pulmonary tissues. a) Uniform manifold approximation and projection (UMAP) for the cell populations subclustered from the whole population of $CD34^{+}CD45^{-}$ pulmonary cells and violin plots of the gene expression of the lineage markers in the cell clusters. b) Pseudotemporal trajectories of the cell clusters. c) Immunostaining of the lungs of wild-type mice and healthy humans (n=3). Scale bar=100 µm. d) Fluorescence-activated cell sorting (FACS) of whole lung cells isolated from bleomycin-injected mice, *VE-cadherin*^{cre}*Mgp*$^{flox/flox}$ mice and *Sm22α*^{cre}*Mgp*$^{flox/flox}$ mice (n=6). Mgp: matrix Gla protein; PDGFR: platelet-derived growth factor receptor; Fn1: fibronectin 1; SMMHC: smooth muscle myosin heavy chain; DAPI: 4',6-diamidino-2-phenylindole.

showed that EC-like myofibroblasts were potentially derived from ECs and differentiated into myofibroblasts (figure 4a and c). Strikingly, differential expression revealed lower expression of the endothelial markers VE-cadherin and von Willebrand factor, but higher expression of the myofibroblast markers α-smooth muscle actin, Col3a1 and Fn1 in EC-like myofibroblasts of pulmonary fibrosis samples compared to those of healthy control samples (figure 4b). A decrease of EC differentiation together with an increase of EC-like myofibroblasts and myofibroblasts was also detected in pulmonary fibrosis (figure 4d). The results suggested that EC-like myofibroblasts contributed myofibroblasts to human pulmonary fibrosis.

Cell lineage tracings reveal EC-like myofibroblasts contributing to pulmonary fibrosis

To further determine if endogenous ECs and EC-like myofibroblasts contributed to pulmonary fibrosis, we preformed cell lineage tracings in the mouse model of bleomycin-induced pulmonary fibrosis. We used

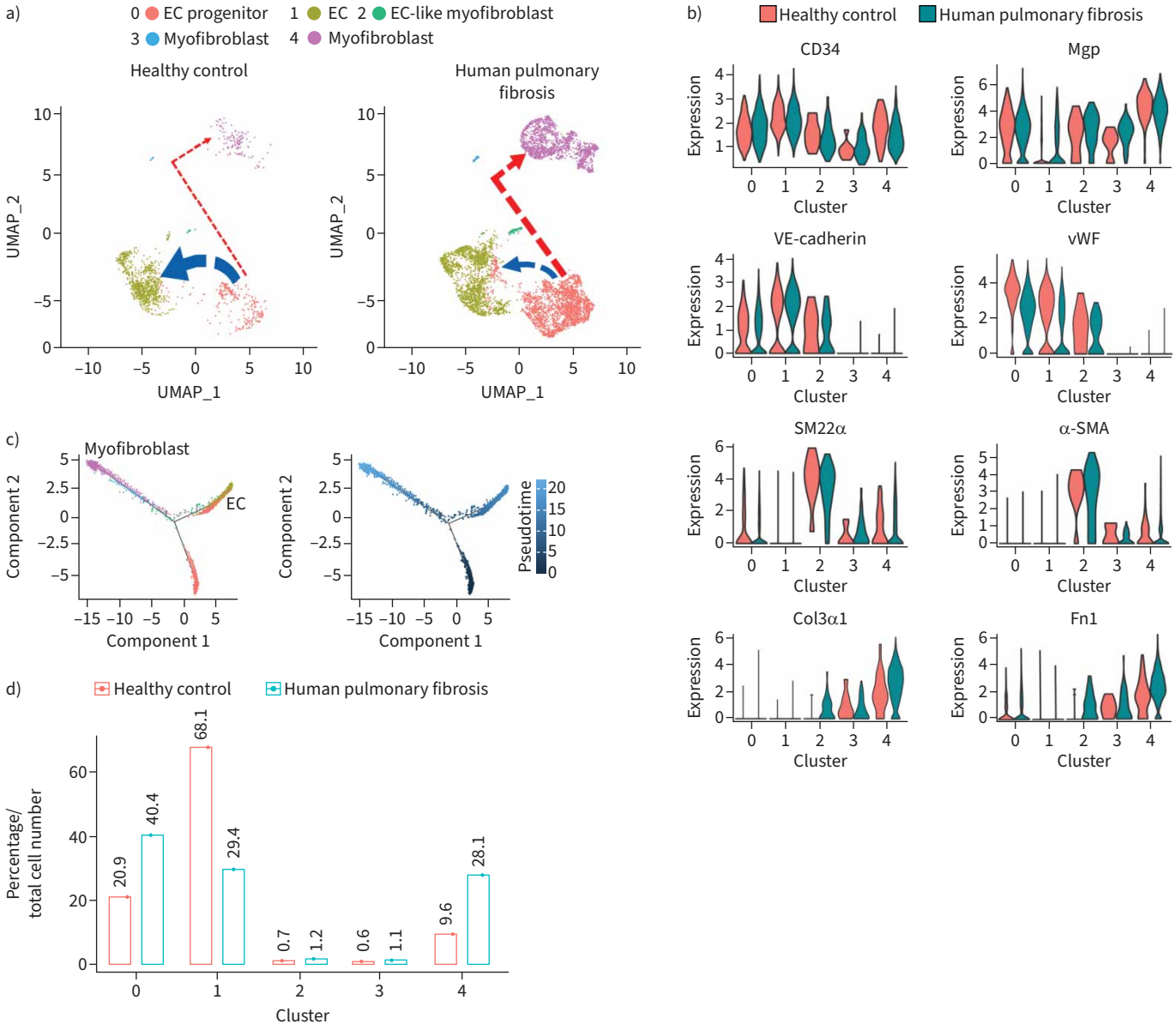

FIGURE 4 Endothelial cell (EC)-like myofibroblasts are present in healthy human lungs and contribute to human pulmonary fibrosis. a) Uniform manifold approximation and projection (UMAP) for cell populations subclustered from the whole population of $CD34^{+}CD45^{-}$ pulmonary cells of healthy human lungs and human pulmonary fibrosis. b) Violin plots of the gene expression of the lineage markers. c) Pseudotemporal trajectories of the cell clusters. d) Alterations in cell compositions of different populations in healthy human lungs and human pulmonary fibrosis. Mgp: matrix Gla protein; vWF: von Willebrand factor; SMA: smooth muscle actin; Fn1: fibronectin 1.

VE-cadherin$^{cre/ERT2}$*Rosa*^{tdTomato} mice where founder cells expressing VE-cadherin could be traced by detecting tdTomato after tamoxifen injections. We also used *SM22α*^{cre}*Rosa*^{tdTomato} mice, in which we could trace the tdTomato-labelled cells that reflected the SM22α expression. At 6 weeks of age, *VE-cadherin*$^{cre/ERT2}$*Rosa*^{tdTomato} mice received tamoxifen injections (75 μg·g^{-1} daily) for five consecutive days to induce tdTomato expression. At 8 weeks of age, tamoxifen-treated *VE-cadherin*$^{cre/ERT2}$*Rosa*^{tdTomato} mice and *SM22α*^{cre}*Rosa*^{tdTomato} mice received bleomycin injections as described previously [48] to induce pulmonary fibrosis. Saline-treated mice were used as controls. At 11 weeks of age, we examined the lung tissues. Masson's trichrome staining showed pulmonary fibrosis in both tamoxifen-treated *VE-cadherin*$^{cre/ERT2}$*Rosa*^{tdTomato} mice and *SM22α*^{cre}*Rosa*^{tdTomato} mice after bleomycin injections (figure 5a and b), confirming the induction of pulmonary fibrosis. In tamoxifen-treated *VE-cadherin*$^{cre/ERT2}$*Rosa*^{tdTomato} mice, immunostaining showed more tdTomato-positive cells expressing higher levels of PDGFRα and Fn1 in the bleomycin-treated group than the controls, suggesting that ECs and EC-like myofibroblasts that expressed VE-cadherin contributed to bleomycin-induced pulmonary fibrosis (figure 5a). In *SM22α*^{cre}*Rosa*^{tdTomato} mice, more tomato-positive cells were identified to express VE-cadherin and a higher level of Fn1 in the bleomycin-treated group than the controls, suggesting again that EC-like myofibroblasts contributed to the bleomycin-induced pulmonary fibrosis (figure 5b).

We bred and examined *SM22α*^{cre}*Rosa*^{tdTomato}*Mgp*$^{flox/flox}$ mice. At 11 weeks of age, we found that more tomato-positive cells expressed VE-cadherin and a higher level of Fn1 than that in *SM22α*^{cre}*Rosa*^{tdTomato} mice (figure 5c). We isolated the tdTomato and VE-cadherin double positive cells from the lungs. Real-time PCR showed higher expression of Col3a1 and Fn1 in the cells isolated from *SM22α*^{cre}*Rosa*^{tdTomato}*Mgp*$^{flox/flox}$ mice than from *SM22α*^{cre}*Rosa*^{tdTomato} mice (figure 5c). Together, multiple cell lineage tracings in the mouse models revealed that EC-like myofibroblasts contributed to pulmonary fibrosis.

MGP controls EC-like myofibroblast differentiation by regulating BMP-1 activity and TGFβ1 maturation

To explore the differentiation of EC-like myofibroblasts in lungs, we isolated tdTomato and VE-cadherin double-positive cells (tdTomato^{+}VE-cadherin^{+}), tdTomato-negative and VE-cadherin-positive cells (tdTomato^{-}VE-cadherin^{+}) and tdTomato-positive and VE-cadherin-negative cells (tdTomato^{+}VE-cadherin^{-}) from the lungs of *SM22α*^{cre}*Rosa*^{tdTomato} mice. We characterised the gene expression of these cells. Real-time PCR showed the expression of MGP, VE-cadherin, SM22α, Col3a1 and Fn1 in tdTomato^{+}VE-cadherin^{+} cells. TdTomato^{-}VE-cadherin^{+} cells expressed VE-cadherin with low level of MGP, but not SM22α, Col3a1 or Fn1. TdTomato^{+}VE-cadherin^{-} expressed MGP, SM22α, Col3a1 and Fn1 and high levels of SMMHC (figure 6a and b). The results suggested that tdTomato^{+}VE-cadherin^{+} cells were the endogenous EC-like myofibroblasts, tdTomato^{-}VE-cadherin^{+} cells were the pulmonary ECs and tdTomato^{+}VE-cadherin^{-} cells could be a mixture of myofibroblasts and smooth muscle cells. We then depleted MGP in these cells using specific siRNA (figure 6c), treated the cells with TGFβ1 (1 ng·mL^{-1}), and examined the myofibroblast markers Col3a1 and Fn1 and endothelial markers VE-cadherin and von Willebrand factor. Real-time PCR showed the induction of myofibroblast markers with the reduction of endothelial markers in MGP-depleted or TGFβ1-treated tdTomato^{+}VE-cadherin^{+} cells. The combination of MGP depletion and excess TGFβ1 significantly magnified the changes in the expression of these markers (figure 6c). The results suggested that lack of MGP or excess TGFβ1 promoted the differentiation of EC-like myofibroblasts toward myofibroblasts. Real-time PCR also showed the induction of myofibroblast markers in MGP-depleted or TGFβ1-treated tdTomato^{+}VE-cadherin^{-} cells and the combination of MGP-depletion and excess TGFβ1 enhanced the induction of these markers (figure 6c), suggesting that lack of MGP or excess TGFβ1 further drove the myofibroblasts towards fibrogenesis. Real-time PCR showed no significant alterations in myofibroblast markers in tdTomato^{-}VE-cadherin^{+} cells. Interestingly, the data showed that TGFβ1 reduced endothelial markers in this cells and MGP depletion further reduced the expression of endothelial markers (figure 6c), suggesting that MGP depletion and excess TGFβ1 caused ECs to lose their identity, but gain potential towards EC-like myofibroblasts.

BMP-1 is known to play a role in the maturation of TGFβ1 [49]. Therefore, we isolated tdTomato^{+}VE-cadherin^{+} cells from the lungs of *SM22α*^{cre}*Rosa*^{tdTomato} mice and treated the cells with BMP-1 in combination with overexpression of FLAG-tagged MGP. Co-immunoprecipitation followed by immunoblotting uncovered an interaction between BMP-1 and MGP (figure 7a). Chemical crosslinking of BMP-1 and FLAG-tagged MGP resulted in the formation of a complex detected by immunoblotting with both anti-FLAG and anti-BMP-1 antibodies (figure 7b), strongly supporting an interaction between BMP-1 and MGP. We used BMP-1 to treat tdTomato^{+}VE-cadherin^{+} cells with or without MGP deletion. The results showed that excess BMP-1 induced Col3a1 and Fn1. With MGP depletion, BMP-1 treatment further induced Col3a1 and Fn1 (figure 7c), suggesting that MGP interfered with the activity of BMP-1.

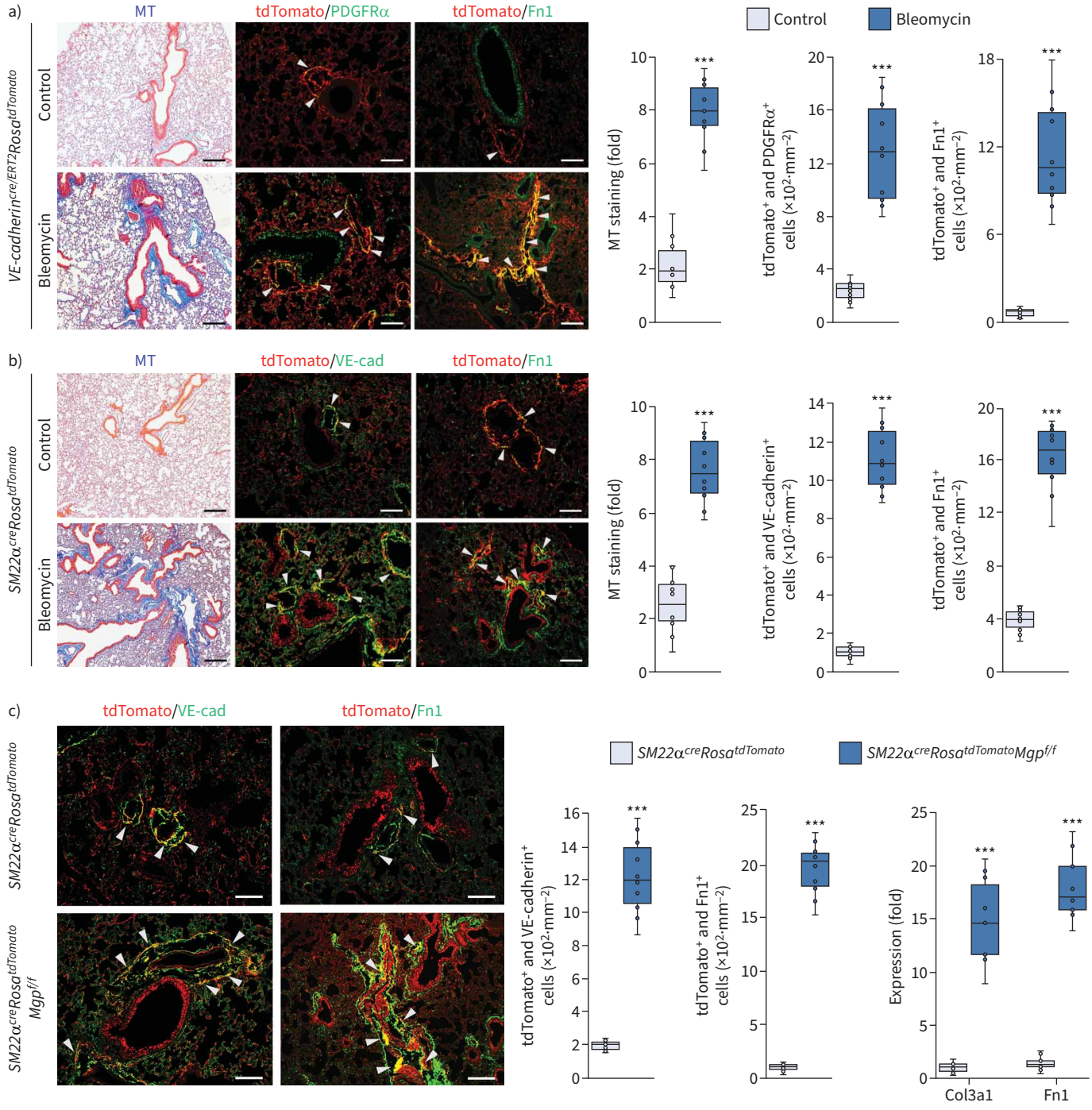

FIGURE 5 Cell lineage tracings reveal endothelial cell (EC)-like myofibroblasts contributing to pulmonary fibrosis. a) Masson's trichrome (MT) staining and immunostaining with cell quantification of the lungs of tamoxifen-injected *VE-cadherin*$^{cre/ERT2}$*Rosa*^{tdTomato} mice after administration of bleomycin (n=10). b) MT staining and immunostaining with cell quantification of the lungs of *Sm22a*^{cre}*Rosa*^{tdTomato} mice after administration of bleomycin (n=10). c) Immunostaining with cell quantification of the lungs of *Sm22a*^{cre}*Rosa*^{tdTomato} and *Sm22a*^{cre}*Rosa*^{tdTomato}*Mgp*$^{Flox/Flox}$ mice. The expression of Col3a1 and fibronectin (Fn)1 in tdTomato and VE-cadherin double-positive cells isolated from lungs of *Sm22a*^{cre}*Rosa*^{tdTomato} and *Sm22a*^{cre}*Rosa*^{tdTomato}*Mgp*$^{Flox/Flox}$ mice (n=10). Scale bars=100 µm. The data were analysed for statistical significance by unpaired two-tailed t-test. The bounds of the boxes are upper and lower quartiles with data points; the line in the box is the median; error bars are maximal and minimal values. PDGFR: platelet-derived growth factor receptor. ***: p<0.0001.

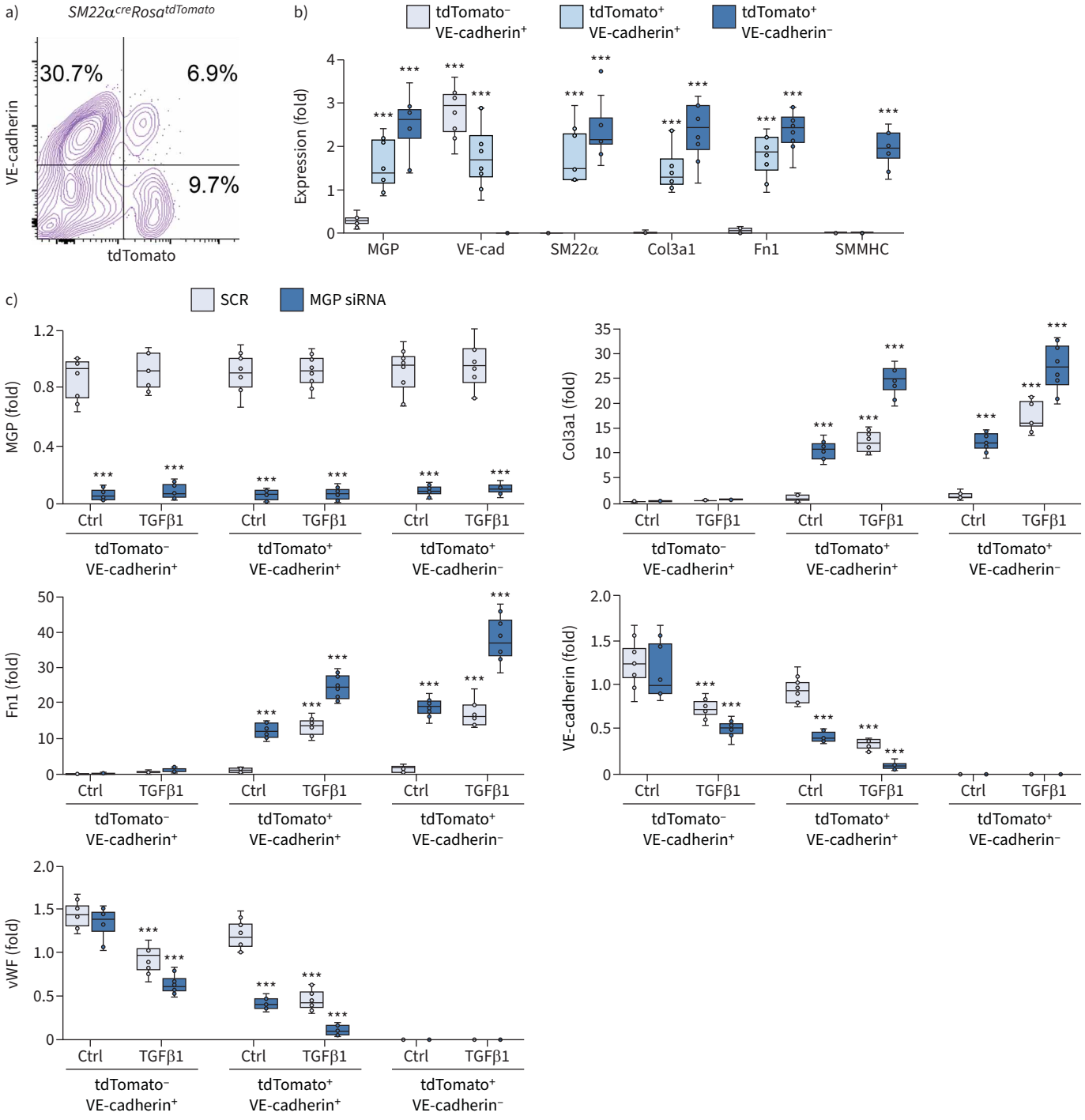

FIGURE 6 Transforming growth factor (TGF)β1 drives endothelial cell (EC)-like myofibroblasts towards myofibroblast differentiation. a) Fluorescence-activated cell sorting of whole lung cells of *Sm22α*^{cre}*Rosa*^{tdTomato} mice. b) Gene expression of tdTomato-negative and VE-cadherin-positive (tdTomato^{-}VE-cadherin^{+}), tdTomato^{+}VE-cadherin^{+} and tdTomato^{+}VE-cadherin^{-} cells isolated from lungs of *Sm22α*^{cre}*Rosa*^{tdTomato} mice (n=6). c) Gene expression of tdTomato^{-}VE-cadherin^{+}, tdTomato^{+}VE-cadherin^{+} and tdTomato^{+}VE-cadherin^{-} cells after matrix Gla protein (MGP) deletion with siRNA and treated with or without *TGFβ1* (1 ng·mL^{-1}) (n=6). Data were analysed for statistical significance by ANOVA with *post hoc* Tukey's test. The bounds of the boxes are upper and lower quartiles with data points; the line in the box is median; error bars are maximal and minimal values. Fn1: fibronectin 1; SMMHC: smooth muscle myosin heavy chain; vWF: von Willebrand factor. ***: p<0.0001.

Since BMP-1 has been shown to cleave LTBP-1 for TGFβ1 maturation [49], we used BMP-1 to treat tdTomato^{+}VE-cadherin^{+} cells with or without the overexpression of MGP and examined LTBP-1 in the cell matrix. Immunoblotting showed that excess BMP-1 efficiently cleaved LTBP-1, and that overexpression of MGP inhibited the BMP-1 cleavage of LTBP-1 (figure 7d). In addition, we determined the levels of TGFβ1

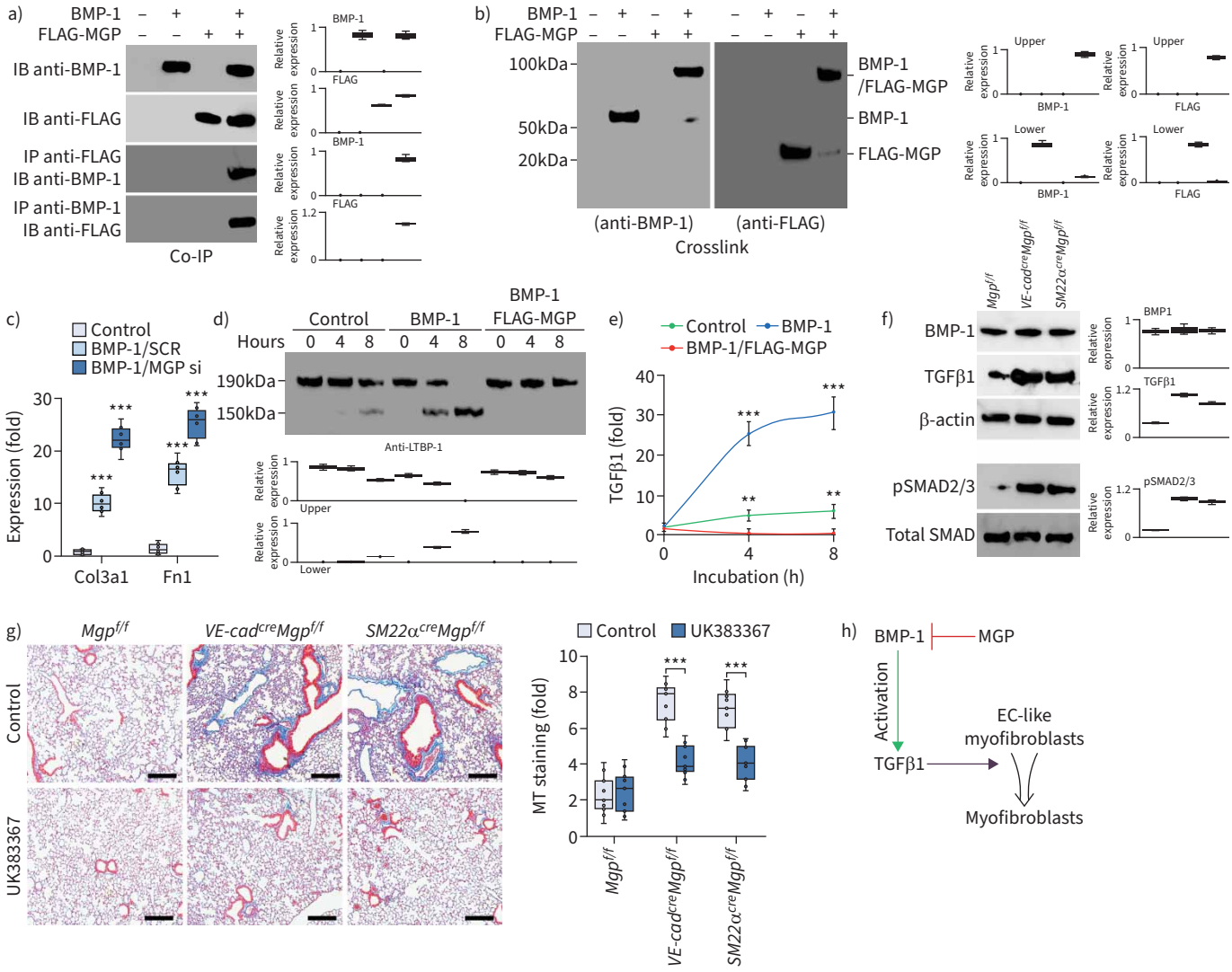

FIGURE 7 Matrix Gla protein (MGP) inhibits bone morphogenic protein (BMP)-1, which regulates maturation of transforming growth factor (TGF)β1 and in turn controls the differentiation of endothelial cell (EC)-like myofibroblasts. a) Binding of BMP-1 to MGP shown by immunoprecipitation. BMP-1 (200 ng) and conditioned medium containing N-FLAG-MGP (100 µL; ~200 ng) were combined as indicated in the top panel, and the presence of the respective protein was confirmed by immunoblotting (IB) (top two blots). Interactions between the proteins were analysed by immunoprecipitation (IP) followed by immunoblotting with antibodies as indicated and quantified by densitometry. b) Binding of BMP-1 to MGP shown by chemical crosslinking. BMP-1 (200 ng) and conditioned medium containing N-FLAG-MGP (100 µL; ~200 ng) were combined as indicated in lane 2 and 3. Interactions were analysed using chemical crosslinking followed by immunoblotting with antibodies as indicated and quantified by densitometry. c) Expression of Col3a1 and Fn1 in tdTomato^{+}VE-cadherin^{+} cells isolated from the lungs of *SM22a^{cre}Rosa^{tdTomato}* mice and treated with BMP-1 (200 ng·mL^{-1}) with transfection of MGP siRNA or scrambled siRNA (SCR) (n=6). d) Time-course immunoblotting with densitometry of latent TGFβ1 binding protein-1 (LTBP-1) in tdTomato^{+}VE-cadherin^{+} cell lysates after treatment with BMP-1 (200 ng·mL^{-1}) with or without conditioned medium containing N-FLAG-MGP (n=6). e) Levels of TGFβ1 in culture media of tdTomato^{+}VE-cadherin^{+} cell after treatment with BMP-1 with or without conditioned medium containing N-FLAG-MGP (n=3). f) Immunoblotting with densitometry of lung tissues of *VE-cadherin^{cre}Mgp$^{flox/flox}$ and Sm22a^{cre}Mgp$^{flox/flox}$* and control mice (n=3). g) Masson's trichrome (MT) staining with quantification of the lungs of *VE-cadherin^{cre}Mgp$^{flox/flox}$* and *Sm22a^{cre}Mgp$^{flox/flox}$* mice and control mice after treatment with UK388367 (n=8). Scale bars=100 µm. h) A schematic representation. c, e and g) were analysed for statistical significance by ANOVA with *post hoc* Tukey's test. The bounds of the boxes are upper and lower quartiles with data points; in c and g) error bars are maximal and minimal values; in e) error bars are mean±SD. **: p<0.001, ***: p<0.0001.

in the media. ELISA showed that BMP-1 increased the TGFβ1 level and that overexpression of MGP decreased the TGFβ1 level, even with BMP-1 treatment (figure 7e). We examined the expression of BMP-1 and TGFβ1 in the lung tissues of *VE-cadherin^{cre}Mgp$^{flox/flox}$* and *SM22α^{cre}Mgp$^{flox/flox}$* mice. Immunoblotting showed higher levels of TGFβ1 in *VE-cadherin^{cre}Mgp$^{flox/flox}$* and *SM22α^{cre}Mgp$^{flox/flox}$* mice than in *Mgp$^{flox/flox}$* control mice (figure 7f). Increased phosphorylation of SMAD2/3 confirmed the induction of TGFβ1 signalling (figure 7f). No change in BMP-1 expression was detected, supporting that the interaction between MGP and BMP-1 inhibited the BMP-1 activity. To determine whether inhibition of BMP-1 affected the pulmonary fibrosis in the new mouse models, we treated *VE-cadherin^{cre}Mgp$^{flox/flox}$* and *SM22α^{cre}Mgp$^{flox/flox}$* mice with the BMP-1 inhibitor UK383367 (5 μg·g^{-1}, daily) for 2 weeks. Masson's trichrome staining showed a reduction of pulmonary fibrosis in both *VE-cadherin^{cre}Mgp$^{flox/flox}$* and *SM22α^{cre}Mgp$^{flox/flox}$* mice after the treatment with UK383367 (figure 7g). Together, the results suggested that MGP interacted with BMP-1, inhibited the production of mature TGFβ1 and in turn regulated the differentiation of EC-like myofibroblasts towards myofibroblasts (figure 7h).

Berbamine prevents the shift of EC-like myofibroblasts towards myofibroblasts and ameliorates pulmonary fibrosis in mouse models

In our studies, the scRNA-seq revealed a clear trajectory of cell differentiation from ECs towards EC-like myofibroblasts and myofibroblasts. By analysing the differential gene expression between myofibroblasts and ECs, we identified 537 genes with increased expression and 668 genes with decreased expression using adjusted p-values cutoff <0.01 (figure 8a). These alterations in gene expression detailed the genetic signature of the shift from ECs to myofibroblasts. To identify a compound that prevented this cell shift, we input the differential expression profile into the CMap platform. The CMap platform is generated to connect genetic variants with small-molecule treatments [50, 51]. Using a connectivity score from designed measurements of expression profiles, a query can be made to search CMap for compounds that cause similar genetic perturbations [52–57]. With this advantage, The CMap platform provides a possible approach to identify compounds that modify the transcriptional landscape towards a desired direction of differentiation. To find a compound to reverse the genetic alteration from ECs to myofibroblasts, we input the top 100 differential expression profiles with an opposite direction of alteration to generate a novel query, which allowed the platform to find the compound with the capability to reverse the genetic alteration. CMap identified a small molecule, berbamine, as a potential candidate.

To determine whether berbamine affected the differentiation of EC-like myofibroblasts, we isolated tdTomato^{+}VE-cadherin^{+} cells from the lungs of *SM22a^{cre}Rosa^{tdTomato}* mice. We treated the cells with 20 μM berbamine for 24 h and found a reduction of myofibroblast markers and an increase of endothelial markers (figure 8b). We also depleted MGP in the cells and treated them with berbamine. Real-time PCR showed that berbamine prevented the induction of myofibroblast markers and restored the expression of endothelial markers in MGP-depleted tdTomato^{+}VE-cadherin^{+} cells (figure 8b). The results suggested that berbamine redirected EC-like myofibroblasts back to EC differentiation.

We treated *VE-cadherin^{cre}Mgp$^{flox/flox}$* mice and *SM22α^{cre}Mgp$^{flox/flox}$* mice at 10 weeks of age with berbamine (100 ng·g^{-1}, daily) for 4 weeks. At 14 weeks of age, we scarified the mice and analysed the lungs. Masson's trichrome staining showed that berbamine significantly decreased the pulmonary fibrosis in both mice (figure 8c and d). In addition, real-time PCR of lung tissue showed that the expression of Col3a1 and Fn1 was reduced in the berbamine-treated group compared to saline-treated controls (figure 8d). The results suggested that berbamine reduced pulmonary fibrosis.

To determine whether berbamine affects TGFβ signalling, we isolated tdTomato^{+}VE-cadherin^{+} cells from the lungs of *SM22a^{cre}Rosa^{tdTomato}* mice and treated the cells with berbamine (20 μM). Real-time PCR and immunoblotting both showed that berbamine reduced the expression of the TGFβ1 receptor ALK5 (figure 9a). We used lentiviral vectors containing CMV promoter-driven ALK5 to infect the cells and treated the cells with berbamine. Real-time PCR showed that excess ALK5 restored the induction of Col3a1 and Fn1 in MGP-depleted tdTomato^{+}VE-cadherin^{+} cells (figure 9b), suggesting that berbamine-reduced ALK5 prevented the differentiation of EC-like myofibroblasts to myofibroblasts. Interestingly, excess ALK5 did not affect berbamine-induced endothelial markers (figure 9b), suggesting that berbamine targets an additional factor to drive EC-like myofibroblasts towards EC differentiation.

Berbamine has previously been identified as an inhibitor of calmodulin 1, a calcium channel blocker [58, 59]. We depleted calmodulin 1 in tdTomato^{+}VE-cadherin^{+} cells and found no change in the expression of endothelial or myofibroblast markers (data not shown), suggesting that inhibition of calmodulin 1 was not involved in the redirection of myofibroblasts. Therefore, we screened the expression of transcription factors that were involved in endothelial differentiation. We found that berbamine significantly induced FoxA2

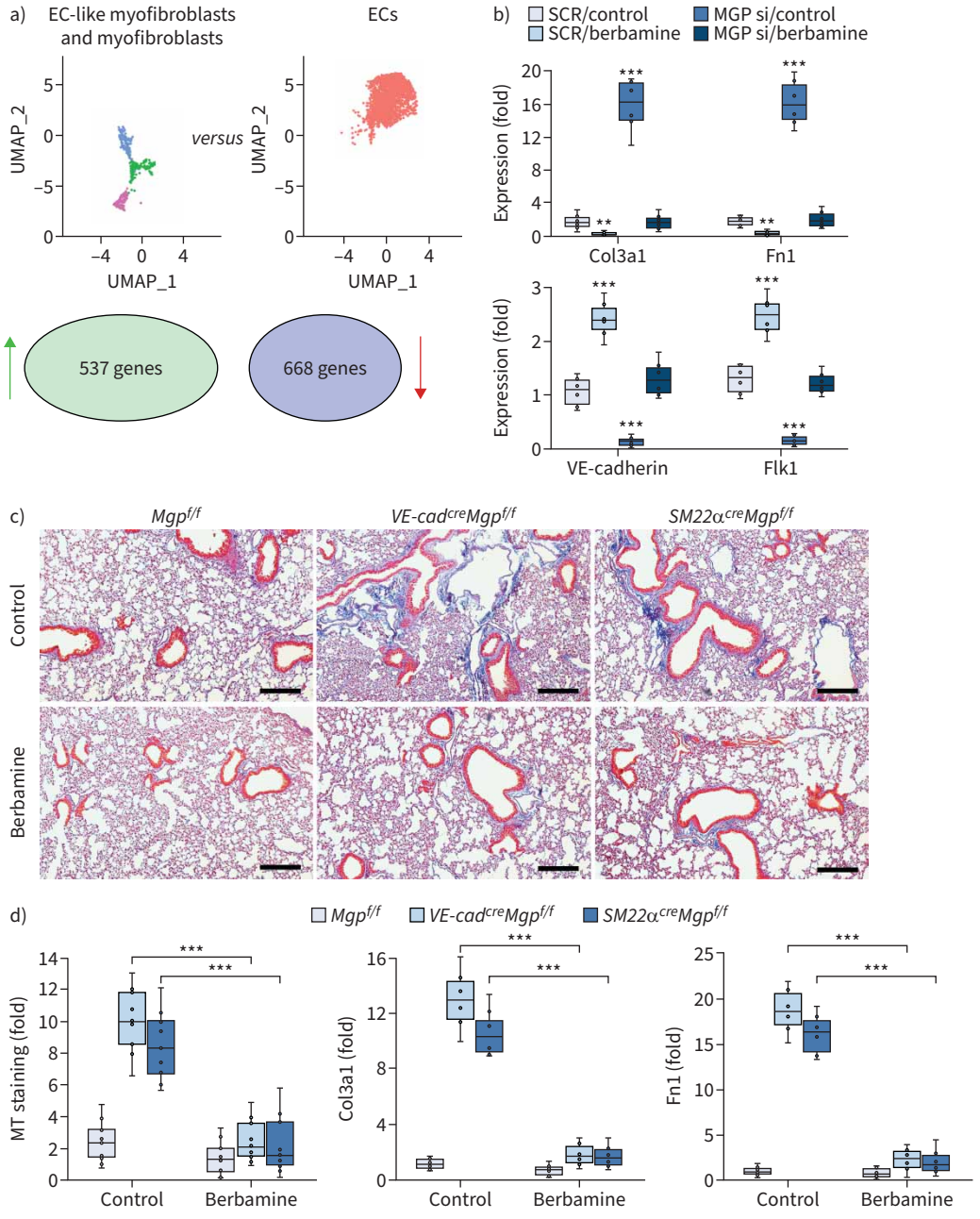

FIGURE 8 Berbamine ameliorates pulmonary fibrosis in mouse models. a) Uniform manifold approximation and projection (UMAP) and differential gene expression between endothelial cell (EC)-like myofibroblasts and ECs. b) Gene expression in tdTomato^{+}VE-cadherin^{+} cells isolated from the lungs of *SM22a^{cre}Rosa^{tdTomato}* mice and treated with berbamine (20 µM) with transfection of matrix Gla protein (MGP) siRNA or scrambled siRNA (SCR) (n=6). c) Masson's trichrome (MT) staining of pulmonary tissues from *VE-cadherin^{cre}Mgp$^{flox/flox}$* and *Sm22a^{cre}Mgp$^{flox/flox}$* mice after berbamine treatment (100 ng·g^{-1}, daily) (n=12). Scale bars=100 µm. d) Quantification of MT staining and expression of Col3a1 and fibronectin 1 (Fn1) in pulmonary tissues from *VE-cadherin^{cre}Mgp$^{flox/flox}$* and *Sm22a^{cre}Mgp$^{flox/flox}$* mice after berbamine treatment (n=9 for quantification of MT and n=6 for gene expression). b) and d) were analysed for statistical significance by ANOVA with *post hoc* Tukey's test. The bounds of the boxes are upper and lower quartiles with data points; the line in the box is median; error bars are maximal and minimal values. **: p<0.001, ***: p<0.0001.

expression (figure 9c) and overexpression of FoxA2 alone reduced the expression of ALK5 and the myofibroblast markers (figure 9d). The combination of berbamine and FoxA2 overexpression further reduced ALK5 and the myofibroblast markers (figure 9d).

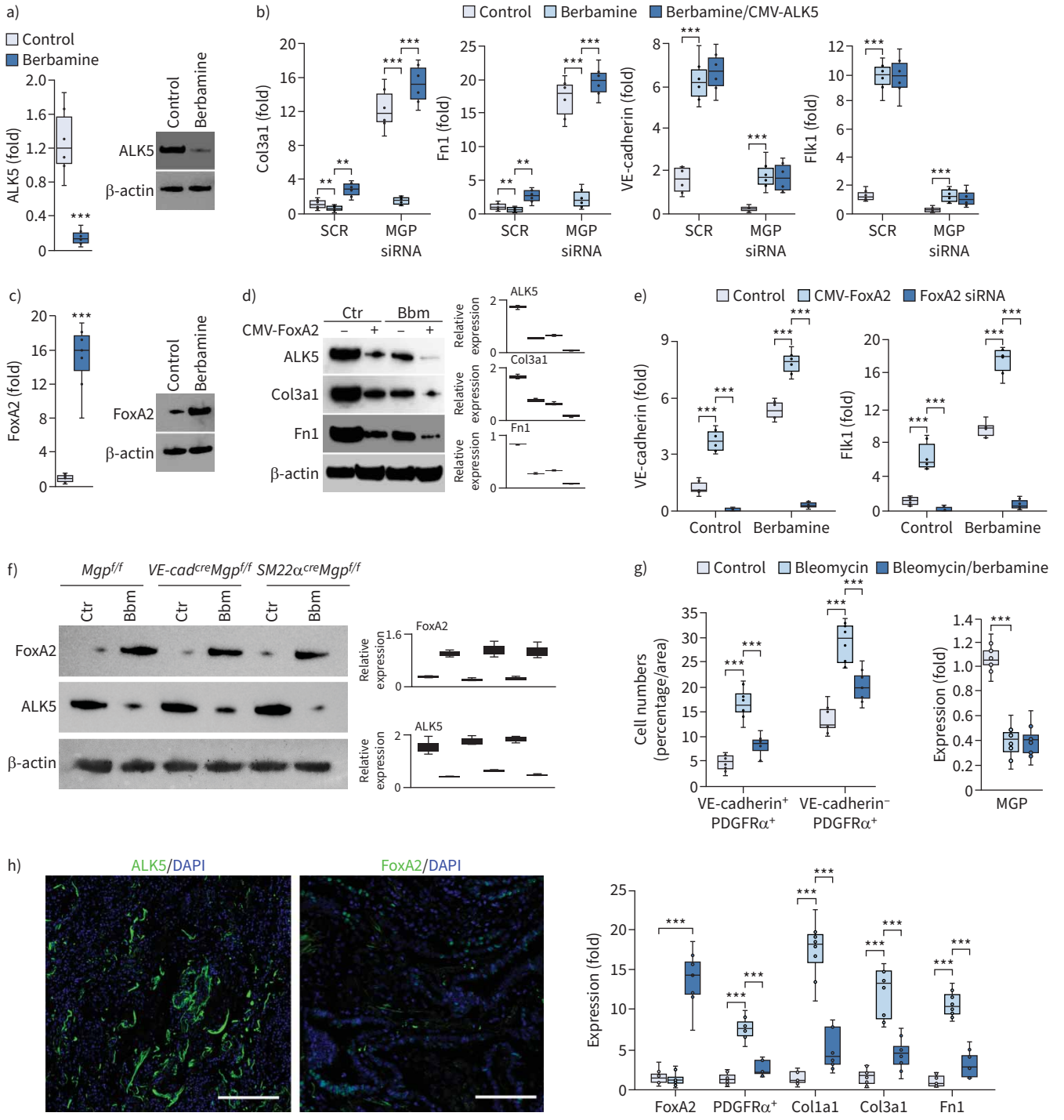

FIGURE 9 Berbamine induces FoxA2 to regulate transforming growth factor (TGF)β signalling and control endothelial cell (EC)-like myofibroblast differentiation. a) Expression of activin receptor-like kinase (ALK)5 in tdTomato^{+}VE-cadherin^{+} cells isolated from the lungs of *SM22a^{cre}Rosa^{tdTomato}* mice and treated with berbamine (20 µM). b) Gene expression in tdTomato^{+}VE-cadherin^{+} cells transfected with matrix Gla protein (MGP) siRNA in combination with berbamine treatment with or without overexpression of ALK5 (n=5). c) Expression of FoxA2 in tdTomato^{+}VE-cadherin^{+} cells isolated from the lungs of *SM22a^{cre}Rosa^{tdTomato}* mice and treated with berbamine (20 µM). d) Immunoblotting with densitometry using tdTomato^{+}VE-cadherin^{+} cell lysates treated with berbamine (Bbm) with or without overexpression of FoxA2 (cytomegalovirus promoter (CMV)-FoxA2) (n=3). e) Expression of endothelial markers in tdTomato^{+}VE-cadherin^{+} cells treated with berbamine in combination with FoxA2 overexpression or FoxA2 knockdown (FoxA2 siRNA) (n=6). f) Immunoblotting with densitometry of the lungs of *VE-cadherin^{cre}Mgp$^{flox/flox}$* mice, *Sm22a^{cre}Mgp$^{flox/flox}$* mice and control mice after treatment of berbamine (Bbm) (n=6). g) Quantification of VE-cadherin-positive and platelet-derived growth factor receptor (PDGFR)α-positive (VE-cadherin^{+}PDGFRα^{+}) cells and VE-cadherin negative and PDGFRα positive (VE-cadherin^{-}PDGFRα^{+}) cells

after immunostaining of the lungs of bleomycin-injected wild-type mice, where gene expression was examined by real-time PCR (n=8). h) Immunostaining of ALK5 and FoxA2 of human pulmonary fibrosis (n=3). Scale bars=100 µm. a) and c) were analysed for statistical significance by unpaired two-tailed t-test. b), e) and g) were analysed for statistical significance by ANOVA with *post hoc* Tukey's test. The bounds of the boxes are upper and lower quartiles with data points; the line in the box is median; error bars are maximal and minimal values. SCR: scrambled siRNA; Ctr: control; Fn1: fibronectin 1. **: p<0.001, ***: p<0.0001.

We overexpressed or depleted FoxA2 in tdTomato^{+}VE-cadherin^{+} cells and treated the cells with berbamine. The results showed that the overexpression of FoxA2 alone induced the endothelial markers (figure 9e). FoxA2 overexpression with berbamine treatment enhanced the induction of endothelial markers whereas FoxA2 depletion abolished the induction of endothelial markers in tdTomatoVE-cadherin^{+} cells (figure 9e). We examined the expression of ALK5 and FoxA2 in the lungs of *VE-cadherin^{cre}Mgp$^{flox/flox}$* mice and *SM22α^{cre}Mgp$^{flox/flox}$* mice after berbamine treatment. Immunoblotting showed that berbamine increased FoxA2 expression and reduced ALK5 expression in the lungs of these mice (figure 9f). We then treated wild-type mice with berbamine (100 ng·g^{-1}, daily) for 4 weeks after bleomycin administration. Berbamine significantly decreased the numbers of both PDGFRα^{+} cells and PDGFRα^{+}VE-cadherin^{+} cells in the lungs of bleomycin-treated mice. Real-time PCR showed a reduction of PDGFRα, Col1a1, Col3a1 and Fn1 (figure 9g). In addition, the results showed that berbamine induced FoxA2, but had no effect on bleomycin-reduced MGP expression (figure 9g). To determine whether ALK5 and FoxA2 were expressed in human pulmonary fibrosis, we performed immunostaining that showed strong expression of ALK5 and less of FoxA2 (figure 9h). Together, these results suggested that berbamine induced FoxA2 to suppress ALK5 expression, in turn redirecting EC-like myofibroblasts towards EC differentiation. The results suggested berbamine as a new treatment strategy for pulmonary fibrosis.

Discussion

Pulmonary fibrosis is a severe fibrotic lung disease with high morbidity and mortality worldwide [1–6]. Although the precise mechanism has not been determined, pulmonary fibrosis is characterised by progressive interstitial fibrogenesis that causes distortion of the alveolar architecture leading to loss of pulmonary function [1–6, 60, 61]. Recent studies have shown ill-fated myofibroblasts emerging in pulmonary fibrosis. These unwanted myofibroblasts are strongly activated during interstitial fibrogenesis, where they produce and deposit excessive amounts of extracellular fibrotic matrix in the tissue [12–20]. In this study, we found that cell-specific deletions of *Mgp* cause pulmonary fibrosis. We showed that MGP regulates the differentiation of a previously unknown population of EC-like myofibroblasts that contributed to the differentiation of myofibroblasts in pulmonary fibrosis. In addition, we identified a small molecule which could redirect the differentiation of the EC-like myofibroblasts and reduce pulmonary fibrosis.

Pulmonary ECs are essential in lung tissue. Endothelial defects result in poor induction of pulmonary lineages from progenitor cells and impaired epithelial repair after lung injury [62]. Pulmonary ECs both support pulmonary epithelial cells and guide their differentiation and maturation [35, 63]. Previous studies have reported co-expression of endothelial and mesenchymal markers in pulmonary disease, suggesting that ECs transition into other lineages under disease conditions [64, 65]. In this study, we uncovered a novel differentiation trajectory in normal lung tissue, where pulmonary ECs may differentiate into EC-like myofibroblasts and ultimately myofibroblasts. We showed that the dysregulation of this differentiation trajectory dramatically increased the production of myofibroblasts that when activated, contributed to pulmonary fibrosis. We found a robust increase of CD34^{+} cells in the lungs of *VE-cadherin^{cre}Mgp$^{flox/flox}$* mice and *SM22α^{cre}Mgp$^{flox/flox}$* mice. We showed CD34 to be expressed in all the cells in the differentiation trajectory, from ECs to myofibroblasts. Additionally, there was an interesting trend of more CD34^{+} cells in *VE-cadherin^{cre}Mgp$^{flox/flox}$* mice than that in *SM22α^{cre}Mgp$^{flox/flox}$* mice (figure 2). The differentiation trajectory projected that ECs were the upstream of EC-like myofibroblasts. Deletion of MGP in ECs could drive more ECs to EC-like myofibroblasts and myofibroblasts than MGP deletion in EC-like myofibroblasts. That would cause more CD34^{+} cells to accumulate in *VE-cadherin^{cre}Mgp$^{flox/flox}$* mice, in which MGP was deleted in ECs and EC-like myofibroblasts, than in *SM22α^{cre}Mgp$^{flox/flox}$* mice, in which MGP was deleted in EC-like myofibroblasts and myofibroblasts.

MGP, a BMP inhibitor, is essential for regulating vascular BMP activity [34, 47, 66–68]. Loss of MGP causes arteriovenous malformation in cerebrum, lungs, kidneys and retina in mice, which resemble the mouse model for hereditary haemorrhagic telangiectasia type 2 [38, 67–69]. Mutations in the human *Mgp* gene cause Keutel syndrome, a rare disease that involves cardiovascular defects and peripheral pulmonary stenoses [39, 70, 71]. However, pulmonary fibrosis has not been reported in these rare patients [39, 70, 71]. In addition, severe side-effects of warfarin treatment in pulmonary fibrosis patients suggest interference by

MGP in pulmonary fibrosis [40–42]. Warfarin inhibits the vitamin K-dependent γ-carboxylation, which is essential for the function of MGP [34]. Warfarin treatment prevents the modification of Glu to Gla residues in MGP, resulting in impaired BMP binding [34]. Warfarin treatment was reported to rapidly worsen the progression of pulmonary fibrosis, and a ban of warfarin in pulmonary fibrosis patents has been suggested [40–42]. In this study, we find that the *Mgp* deletion in VE-cadherin- or SM22α-positive cells causes pulmonary fibrosis in mice, suggesting an important role of MGP in the fibrotic process. These mice provide new animal models for the study of pulmonary fibrosis.

BMP-1 was initially classified as a BMP based on bone induction [72–74]. However, BMP-1 encodes a metalloprotease with few similarities to other BMPs, and is not included in the TGFβ superfamily of growth factors [75]. BMP-1 executes its activity by modifying the protein precursors to mature proteins [75–77]. For example, BMP-1 cleaves the BMP antagonist Chordin to regulate BMP activity [78]. BMP-1 also processes extracellular matrix proteins such as collagens, biglycan and osteoglycin [77, 79]. Interestingly, fibroblasts strongly increase the deposition of collagens onto the insoluble extracellular matrix when incubated with BMP-1 [80]. In addition, BMP-1 cleaves LTBP-1 to facilitate the maturation of TGFβ1, a master regulator of myofibroblast differentiation in pulmonary fibrosis [49]. Our study suggests that MGP binds to BMP-1 and reduces the production of mature TGFβ1, thereby regulating the differentiation of EC-like myofibroblasts to myofibroblasts. We showed that inhibition of BMP-1 decreased the fibrosis in the lungs of *VE-cadherin*^{cre}*Mgp*$^{flox/flox}$ mice and *SM22α*^{cre}*Mgp*$^{flox/flox}$ mice. The deletion of BMP-1 was unable to reduce bleomycin-induced pulmonary fibrosis [81], which indicated the mechanism of fibrosis in *VE-cadherin*^{cre}*Mgp*$^{flox/flox}$ mice and *SM22α*^{cre}*Mgp*$^{flox/flox}$ mice may differ from bleomycin-induced fibrosis. The precise mechanism of bleomycin-induced fibrosis is yet to be revealed. Previous studies uncovered that bleomycin injured lung cells and triggered the influx of inflammatory and immune cells, which may lead to fibrogenesis [82]. To our knowledge, no studies have shown whether BMP-1 is involved in the inflammatory response towards fibrogenesis. The fibrosis in *VE-cadherin*^{cre}*Mgp*$^{flox/flox}$ mice and *SM22α*^{cre}*Mgp*$^{flox/flox}$ mice occurred during development and we did not observe accumulation of inflammatory cells in the lungs of these mice. During lung development, BMP-1 acts as an important factor for TGFβ1 production, which is essential to balance the differentiation of ECs and myofibroblasts [49, 83]. We argue that lack of MGP unleashes BMP-1 activity, enhances the production of mature TGFβ1, pushes ECs and EC-like myofibroblasts towards myofibroblast differentiation, subsequently causing fibrosis.

Our results suggested an interaction between MGP and BMP-1. MGP has been shown to bind to BMP-2, -4 and -7 through Proline-64 and surrounding Gla residues [34]. MGP has also been shown to interact with several other proteins, such as Fn1 and vitronectin through its C-terminus [84, 85] and elastin with its N-terminus [86]. Further studies would be necessary to identify what region of MGP interacts with BMP-1. The balance between BMP-1 activity and other BMPs regulated by MGP would also be interesting to explore in fibrosis. Since BMP-1 is a metalloprotease, the effect of BMP-1 on fibrosis would be different from that of other BMPs. Some BMPs are reported to reduce fibrogenesis through suppression of TGFβ signalling [87], but our results suggest that enhanced BMP-1 activity increases TGFβ1 signalling to cause fibrosis. Differences in affinity between MGP and various BMPs might also be important to explain variations in BMPs' activity after loss of MGP. The complexity of extracellular cell matrix may also play an important role.

Berbamine is a small molecule extracted from the plant named berberis [88]. Berbamine was initially identified as a calcium channel blocker with anti-arrhythmic effects and ischaemic protective activity through the inhibition of calmodulin 1 [58, 59]. Recent studies also found that berbamine inhibits the NF-κB signalling pathway for antimyeloma effects and reduces the activity of signal transducer and activator of transcription 3 in hepatocellular carcinoma [89, 90]. Our results showed that berbamine induced the transcription factor FoxA2, which not only prevented EC-like myofibroblasts from differentiating into myofibroblasts, but also shifted EC-like myofibroblasts towards ECs. FoxA2 is essential for the development of the cardiovascular system [91]. FoxA2 is highly expressed at an early stage of EC differentiation and the progenitors of FoxA2^{+} endoderm contribute ECs [92, 93]. Therefore, it is not surprising that FoxA2 induced by berbamine redirected EC-like myofibroblasts back to EC differentiation, decreasing myofibroblasts and fibrosis.

Author contributions: Yucheng Yao supervised the experiments, analysed data and wrote the manuscript. Xiuju Wu, Daoqin Zhang, Xiaojing Qiao, Li Zhang, Xinjiang Cai, Jaden Ji, Jocelyn A. Ma, Yan Zhao, John A. Belperio and Kristina I. Boström performed experiments and data analysis.

Conflict of interest: The authors have no potential conflicts of interest to disclose.

Support statement: Funding for this work was provided in part by National Institutes of Health grants NS79353, HL139675 and HL162643 (to Yucheng Yao), and HL81397 and HL154548 (to Kristina I. Boström). Funding information for this article has been deposited with the Crossref Funder Registry.

References

1 Hutchinson J, Fogarty A, Hubbard R, *et al.* Global incidence and mortality of idiopathic pulmonary fibrosis: a systematic review. *Eur Respir J* 2015; 46: 795–806.
2 Lederer DJ, Martinez FJ. Idiopathic pulmonary fibrosis. *N Engl J Med* 2018; 379: 797–798.
3 Martinez FJ, Collard HR, Pardo A, *et al.* Idiopathic pulmonary fibrosis. *Nat Rev Dis Primers* 2017; 3: 17074.
4 Raghu G, Collard HR, Egan JJ, *et al.* An official ATS/ERS/JRS/ALAT statement: idiopathic pulmonary fibrosis: evidence-based guidelines for diagnosis and management. *Am J Respir Crit Care Med* 2011; 183: 788–824.
5 Raghu G, Weycker D, Edelsberg J, *et al.* Incidence and prevalence of idiopathic pulmonary fibrosis. *Am J Respir Crit Care Med* 2006; 174: 810–816.
6 Richeldi L, Collard HR, Jones MG. Idiopathic pulmonary fibrosis. *Lancet* 2017; 389: 1941–1952.
7 Barratt SL, Creamer A, Hayton C, *et al.* Idiopathic pulmonary fibrosis (IPF): an overview. *J Clin Med* 2018; 7: 201.
8 Hamanaka RB, Mutlu GM. Metabolic requirements of pulmonary fibrosis: role of fibroblast metabolism. *FEBS J* 2021; 288: 6331–6352.
9 Kim HJ, Perlman D, Tomic R. Natural history of idiopathic pulmonary fibrosis. *Respir Med* 2015; 109: 661–670.
10 Hewson T, McKeever TM, Gibson JE, *et al.* Timing of onset of symptoms in people with idiopathic pulmonary fibrosis. *Thorax* 2018; 73: 683–685.
11 Ley B, Ryerson CJ, Vittinghoff E, *et al.* A multidimensional index and staging system for idiopathic pulmonary fibrosis. *Ann Intern Med* 2012; 156: 684–691.
12 King TE Jr, Pardo A, Selman M. Idiopathic pulmonary fibrosis. *Lancet* 2011: 378: 1949–1961.
13 Tsukui T, Sun KH, Wetter JB, *et al.* Collagen-producing lung cell atlas identifies multiple subsets with distinct localization and relevance to fibrosis. *Nat Commun* 2020; 11: 1920.
14 Valenzi E, Bulik M, Tabib T, *et al.* Single-cell analysis reveals fibroblast heterogeneity and myofibroblasts in systemic sclerosis-associated interstitial lung disease. *Ann Rheum Dis* 2019; 78: 1379–1387.
15 Peyser R, MacDonnell S, Gao Y, *et al.* Defining the activated fibroblast population in lung fibrosis using single-cell sequencing. *Am J Respir Cell Mol Biol* 2019; 61: 74–85.
16 Pakshir P, Noskovicova N, Lodyga M, *et al.* The myofibroblast at a glance. *J Cell Sci* 2020; 133: jcs227900.
17 Phan SH. Genesis of the myofibroblast in lung injury and fibrosis. *Proc Am Thorac Soc* 2012; 9: 148–152.
18 Phan SH. The myofibroblast in pulmonary fibrosis. *Chest* 2002; 122: Suppl. 6, 286S–289S.
19 Xie T, Wang Y, Deng N, *et al.* Single-cell deconvolution of fibroblast heterogeneity in mouse pulmonary fibrosis. *Cell Rep* 2018; 22: 3625–3640.
20 Habiel DM, Hogaboam CM. Heterogeneity of fibroblasts and myofibroblasts in pulmonary fibrosis. *Curr Pathobiol Rep* 2017; 5: 101–110.
21 Uhal BD, Joshi I, Hughes WF, *et al.* Alveolar epithelial cell death adjacent to underlying myofibroblasts in advanced fibrotic human lung. *Am J Physiol* 1998; 275: L1192–L1199.
22 Jablonski RP, Kim SJ, Cheresh P, *et al.* SIRT3 deficiency promotes lung fibrosis by augmenting alveolar epithelial cell mitochondrial DNA damage and apoptosis. *FASEB J* 2017; 31: 2520–2532.
23 Misharin AV, Morales-Nebreda L, Reyfman PA, *et al.* Monocyte-derived alveolar macrophages drive lung fibrosis and persist in the lung over the life span. *J Exp Med* 2017; 214: 2387–2404.
24 Naikawadi RP, Disayabutr S, Mallavia B, *et al.* Telomere dysfunction in alveolar epithelial cells causes lung remodeling and fibrosis. *JCI Insight* 2016; 1: e86704.
25 Gabbiani G, Hirschel BJ, Ryan GB, *et al.* Granulation tissue as a contractile organ. A study of structure and function. *J Exp Med* 1972; 135: 719–734.
26 Gabbiani G, Ryan GB, Majne G. Presence of modified fibroblasts in granulation tissue and their possible role in wound contraction. *Experientia* 1971; 27: 549–550.
27 Majno G, Gabbiani G, Hirschel BJ, *et al.* Contraction of granulation tissue *in vitro*: similarity to smooth muscle. *Science* 1971; 173: 548–550.
28 Darby I, Skalli O, Gabbiani G. Alpha-smooth muscle actin is transiently expressed by myofibroblasts during experimental wound healing. *Lab Invest* 1990; 63: 21–29.
29 Karin D, Koyama Y, Brenner D, *et al.* The characteristics of activated portal fibroblasts/myofibroblasts in liver fibrosis. *Differentiation* 2016; 92: 84–92.
30 Di Carlo SE, Peduto L. The perivascular origin of pathological fibroblasts. *J Clin Invest* 2018; 128: 54–63.
31 Tallquist MD, Molkentin JD. Redefining the identity of cardiac fibroblasts. *Nat Rev Cardiol* 2017; 14: 484–491.
32 Adams TS, Schupp JC, Poli S, *et al.* Single-cell RNA-seq reveals ectopic and aberrant lung-resident cell populations in idiopathic pulmonary fibrosis. *Sci Adv* 2020; 6: eaba1983.
33 Reyfman PA, Walter JM, Joshi N, *et al.* Single-cell transcriptomic analysis of human lung provides insights into the pathobiology of pulmonary fibrosis. *Am J Respir Crit Care Med* 2019; 199: 1517–1536.

34 Yao Y, Shahbazian A, Bostrom KI. Proline and γ-carboxylated glutamate residues in matrix Gla protein are critical for binding of bone morphogenetic protein-4. *Circ Res* 2008; 102: 1065–1074.
35 Yao J, Guihard PJ, Wu X, *et al.* Vascular endothelium plays a key role in directing pulmonary epithelial cell differentiation. *J Cell Biol* 2017; 216: 3369–3385.
36 Yao Y, Nowak S, Yochelis A, *et al.* Matrix GLA protein, an inhibitory morphogen in pulmonary vascular development. *J Biol Chem* 2007; 282: 30131–30142.
37 Gilbert KA, Rannels SR. Matrix GLA protein modulates branching morphogenesis in fetal rat lung. *Am J Physiol Lung Cell Mol Physiol* 2004; 286: L1179–L1187.
38 Yao Y, Jumabay M, Wang A, *et al.* Matrix Gla protein deficiency causes arteriovenous malformations in mice. *J Clin Invest* 2011; 121: 2993–3004.
39 Meier M, Weng LP, Alexandrakis E, *et al.* Tracheobronchial stenosis in Keutel syndrome. *Eur Respir J* 2001; 17: 566–569.
40 Alagha K, Secq V, Pahus L, *et al.* We should prohibit warfarin in idiopathic pulmonary fibrosis. *Am J Respir Crit Care Med* 2015; 191: 958–960.
41 Cottin V, Crestani B, Valeyre D, *et al.* Recommandations pratiques pour le diagnostic et la prise en charge de la fibrose pulmonaire idiopathique. Élaborées par le centre national de référence et les centres de compétence pour les maladies pulmonaires rares sous l'égide de la Société de Pneumologie de Langue Française. [French practical guidelines for the diagnosis and management of idiopathic pulmonary fibrosis. From the National Reference and the Competence centers for rare diseases and the Société de Pneumologie de Langue Francaise]. *Rev Mal Respir* 2013; 30: 879–902.
42 Noth I, Anstrom KJ, Calvert SB, *et al.* A placebo-controlled randomized trial of warfarin in idiopathic pulmonary fibrosis. *Am J Respir Crit Care Med* 2012; 186: 88–95.
43 Yao J, Guihard PJ, Blazquez-Medela AM, *et al.* Matrix Gla protein regulates differentiation of endothelial cells derived from mouse embryonic stem cells. *Angiogenesis* 2016; 19: 1–7.
44 Yao Y, Jumabay M, Ly A, *et al.* A role for the endothelium in vascular calcification. *Circ Res* 2013; 113: 495–504.
45 Yao J, Guihard PJ, Blazquez-Medela AM, *et al.* Serine protease activation essential for endothelial-mesenchymal transition in vascular calcification. *Circ Res* 2015; 117: 758–769.
46 National Research Council. Guide for the Care and Use of Laboratory Animals. 8th Edn. Washington, National Academies Press, 2011.
47 Yao Y, Zebboudj AF, Shao E, *et al.* Regulation of bone morphogenetic protein-4 by matrix GLA protein in vascular endothelial cells involves activin-like kinase receptor 1. *J Biol Chem* 2006; 281: 33921–33930.
48 Harrison JH Jr, Lazo JS. High dose continuous infusion of bleomycin in mice: a new model for drug-induced pulmonary fibrosis. *J Pharmacol Exp Ther* 1987; 243: 1185–1194.
49 Ge G, Greenspan DS. BMP1 controls TGFβ1 activation *via* cleavage of latent TGFβ-binding protein. *J Cell Biol* 2006; 175: 111–120.
50 Subramanian A, Narayan R, Corsello SM, *et al.* A next generation connectivity map: L1000 platform and the first 1,000,000 profiles. *Cell* 2017; 171: 1437–1452.
51 Duan Q, Flynn C, Niepel M, *et al.* LINCS Canvas Browser: interactive web app to query, browse and interrogate LINCS L1000 gene expression signatures. *Nucleic Acids Res* 2014; 42: W449–W460.
52 Qiu Y, Lu T, Lim H, *et al.* A Bayesian approach to accurate and robust signature detection on LINCS L1000 data. *Bioinformatics* 2020; 36: 2787–2795.
53 Liu TP, Hsieh YY, Chou CJ, *et al.* Systematic polypharmacology and drug repurposing *via* an integrated L1000-based Connectivity Map database mining. *R Soc Open Sci* 2018; 5: 181321.
54 Brum AM, van de Peppel J, van der Leije CS, *et al.* Connectivity Map-based discovery of parbendazole reveals targetable human osteogenic pathway. *Proc Natl Acad Sci USA* 2015; 112: 12711–12716.
55 Dyle MC, Ebert SM, Cook DP, *et al.* Systems-based discovery of tomatidine as a natural small molecule inhibitor of skeletal muscle atrophy. *J Biol Chem* 2014; 289: 14913–14924.
56 Farooq F, Balabanian S, Liu X, *et al.* p38 Mitogen-activated protein kinase stabilizes SMN mRNA through RNA binding protein HuR. *Hum Mol Genet* 2009; 18: 4035–4045.
57 Liu J, Lee J, Salazar Hernandez MA, *et al.* Treatment of obesity with celastrol. *Cell* 2015; 161: 999–1011.
58 Xu CQ, Dong DL, Du ZM, *et al.* [Comparison of the anti-arrhythmic effects of matrine and berbamine with amiodarone and RP58866]. *Yao Xue Xue Bao* 2004; 39: 691–694.
59 Guo ZB, Cao HY, Xu Z, *et al.* [Electrophysiological effects of berbamine on ischemic ventricular tachyarrhythmia]. *Zhongguo Yao Li Xue Bao* 1991; 12: 44–47.
60 Wolters PJ, Collard HR, Jones KD. Pathogenesis of idiopathic pulmonary fibrosis. *Annu Rev Pathol* 2014; 9: 157–179.
61 Selman M, Pardo A. Revealing the pathogenic and aging-related mechanisms of the enigmatic idiopathic pulmonary fibrosis. An integral model. *Am J Respir Crit Care Med* 2014; 189: 1161–1172.
62 Lee J-H, Bhang DH, Beede A, *et al.* Lung stem cell differentiation in mice directed by endothelial cells *via* a BMP4-NFATc1-thrombospondin-1 axis. *Cell* 2014; 156: 440–455.
63 Ding BS, Nolan DJ, Guo P, *et al.* Endothelial-derived angiocrine signals induce and sustain regenerative lung alveolarization. *Cell* 2011; 147: 539–553.

64 El Agha E, Kramann R, Schneider RK, *et al.* Mesenchymal stem cells in fibrotic disease. *Cell Stem Cell* 2017; 21: 166–177.
65 Lemos DR, Duffield JS. Tissue-resident mesenchymal stromal cells: implications for tissue-specific antifibrotic therapies. *Sci Transl Med* 2018; 10: eaan5174.
66 Yao Y, Zebboudj AF, Torres A, *et al.* Activin-like kinase receptor 1 (ALK1) in atherosclerotic lesions and vascular mesenchymal cells. *Cardiovasc Res* 2007; 74: 279–289.
67 Guihard PJ, Guo Y, Wu X, *et al.* Shaping waves of bone morphogenetic protein inhibition during vascular growth. *Circ Res* 2020; 127: 1288–1305.
68 Boström KI, Guihard P, Blazquez Medela AM, *et al.* Matrix Gla protein limits pulmonary arteriovenous malformations in ALK1 deficiency. *Eur Respir J* 2015; 45: 849–852.
69 Yao Y, Yao J, Radparvar M, *et al.* Reducing Jagged 1 and 2 levels prevents cerebral arteriovenous malformations in matrix Gla protein deficiency. *Proc Natl Acad Sci USA* 2013; 110: 19071–19076.
70 Keutel J, Jörgensen G, Gabriel P. Ein neues autosomal-rezessiv vererbbares Syndrom. Multiple periphere Pulmonalstenosen, Brachytelephalangie, Innenohrschwerhörigkeit, Knorpelverknöcherungen bzw. -Verkalkungen. [A new autosomal-recessive hereditary syndrome. Multiple peripheral pulmonary stenosis, brachytelephalangia, inner-ear deafness, ossification or calcification of cartilages]. *Dtsch Med Wochenschr* 1971; 96: 1676–1681.
71 Cancela ML, Laizé V, Conceição N, *et al.* Keutel syndrome, a review of 50 years of literature. *Front Cell Dev Biol* 2021; 9: 642136.
72 Wozney JM. Bone morphogenetic proteins. *Prog Growth Factor Res* 1989; 1: 267–280.
73 Wozney JM, Rosen V, Celeste AJ, *et al.* Novel regulators of bone formation: molecular clones and activities. *Science* 1988; 242: 1528–1534.
74 Tabas JA, Zasloff M, Wasmuth JJ, *et al.* Bone morphogenetic protein: chromosomal localization of human genes for BMP1, BMP2A, and BMP3. *Genomics* 1991; 9: 283–289.
75 Kessler E, Takahara K, Biniaminov L, *et al.* Bone morphogenetic protein-1: the type I procollagen C-proteinase. *Science* 1996; 271: 360–362.
76 Mac Sweeney A, Gil-Parrado S, Vinzenz D, *et al.* Structural basis for the substrate specificity of bone morphogenetic protein 1/tolloid-like metalloproteases. *J Mol Biol* 2008; 384: 228–239.
77 Scott IC, Blitz IL, Pappano WN, *et al.* Mammalian BMP-1/Tolloid-related metalloproteinases, including novel family member mammalian Tolloid-like 2, have differential enzymatic activities and distributions of expression relevant to patterning and skeletogenesis. *Dev Biol* 1999; 213: 283–300.
78 Piccolo S, Sasai Y, Lu B, *et al.* Dorsoventral patterning in *Xenopus*: inhibition of ventral signals by direct binding of chordin to BMP-4. *Cell* 1996; 86: 589–598.
79 Uzel MI, Scott IC, Babakhanlou-Chase H, *et al.* Multiple bone morphogenetic protein 1-related mammalian metalloproteinases process pro-lysyl oxidase at the correct physiological site and control lysyl oxidase activation in mouse embryo fibroblast cultures. *J Biol Chem* 2001; 276: 22537–22543.
80 Rosell-Garcia T, Rodriguez-Pascual F. Enhancement of collagen deposition and cross-linking by coupling lysyl oxidase with bone morphogenetic protein-1 and its application in tissue engineering. *Sci Rep* 2018; 8: 10780.
81 Ma HY, N'Diaye EN, Caplazi P, *et al.* BMP1 is not required for lung fibrosis in mice. *Sci Rep* 2022; 12: 5466.
82 Hay J, Shahzeidi S, Laurent G. Mechanisms of bleomycin-induced lung damage. *Arch Toxicol* 1991; 65: 81–94.
83 Goumans MJ, Liu Z, ten Dijke P. TGF-beta signaling in vascular biology and dysfunction. *Cell Res* 2009; 19: 116–127.
84 Nishimoto SK, Nishimoto M. Matrix gla protein binds to fibronectin and enhances cell attachment and spreading on fibronectin. *Int J Cell Biol* 2014; 2014: 807013.
85 Dufourcq P, Louis H, Moreau C, *et al.* Vitronectin expression and interaction with receptors in smooth muscle cells from human atheromatous plaque. *Arterioscler Thromb Vasc Biol* 1998; 18: 168–176.
86 Parashar A, Gourgas O, Lau K, *et al.* Elastin calcification in *in vitro* models and its prevention by MGP's N-terminal peptide. *J Struct Biol* 2021; 213: 107637.
87 Yang G, Zhu Z, Wang Y, *et al.* Bone morphogenetic protein 7 attenuates epithelial-mesenchymal transition induced by silica. *Hum Exp Toxicol* 2016; 35: 69–77.
88 Schiff PL Jr. Bisbenzylisoquinoline alkaloids. *J Nat Prod* 1991; 54: 645–749.
89 Liang Y, Xu RZ, Zhang L, *et al.* Berbamine, a novel nuclear factor κB inhibitor, inhibits growth and induces apoptosis in human myeloma cells. *Acta Pharmacol Sin* 2009; 30: 1659–1665.
90 Zhao W, Bai B, Hong Z, *et al.* Berbamine (BBM), a natural STAT3 inhibitor, synergistically enhances the antigrowth and proapoptotic effects of sorafenib on hepatocellular carcinoma cells. *ACS Omega* 2020; 5: 24838–24847.
91 Bardot E, Calderon D, Santoriello F, *et al.* Foxa2 identifies a cardiac progenitor population with ventricular differentiation potential. *Nat Commun* 2017; 8: 14428.
92 Pak B, Schmitt CE, Choi W, *et al.* Analyses of avascular mutants reveal unique transcriptomic signature of non-conventional endothelial cells. *Front Cell Dev Biol* 2020; 8: 589717.
93 Madeddu P. FoxA2 hunting research identifies the early trail of mesenchymal differentiation. *Stem Cell Res Ther* 2013; 4: 40.